Correction (1 June 2011): The two tables had been inadvertently omitted from the original version of this supplement.

www.sciencemag.org/cgi/content/full/science.1206731/DC1

Supporting Online Material for

The 2011 Magnitude 9.0 Tohoku-Oki Earthquake: Mosaicking the Megathrust from Seconds to Centuries

Mark Simons,* Sarah E. Minson, Anthony Sladen, Francisco Ortega, Junle Jiang, Susan E. Owen, Lingsen Meng, Jean-Paul Ampuero, Shengji Wei, Risheng Chu, Donald V. Helmberger, Hiroo Kanamori, Eric Hetland, Angelyn W. Moore, Frank H. Webb

*To whom correspondence should be addressed. E-mail: simons@caltech.edu

Published 19 May 2011 on *Science* Express
DOI: 10.1126/science.1206731

This PDF file includes:

SOM Text

GPS Processing

The 5-minute position estimates were calculated using Jet Propulsion Laboratory's GIPSY-OASIS software (*35*). We use a single-station bias-fixed point positioning (*36*) and kinematic positioning strategy. For the kinematic positioning, the station position is a stochastic parameter in the model used to fit the GPS observations. Using the point-positioning technique, the GPS orbit and clock estimates, provided by JPL's GPS Analysis Center, are held fixed. The resulting positions are therefore not relative to any site, which allows the results to be free of common mode errors introduced into double differenced high rate positions (*37*). Troposphere zenith delay and gradients were also estimated as stochastic parameters in our analysis.

To calculate the coseismic offsets, we use the time series sampled at 5-minute intervals in the time period of 2 hours before and after the time of the mainshock. For each component (north, east, up) of each time series, we fit the time series for a constant and two step functions – one for the mainshock and one for the aftershock, plus a linear post-seismic for the mainshock. To estimate errors on the coseismic jumps, we rescale the formal errors on the GPS time series using the RMS of the residuals after removing the constant and jumps. In the finite fault modeling, we then inflate the GPS errors further by a factor of 4 in order to account for systematic errors such as inaccuracies in the assumed elastic structure or the geometry of the fault.

Each component of the GPS positional data is modeled as follows:

$$d(t) = C_0 + M_C \cdot H(t - t_M) + M_P \cdot (t - t_M) \cdot H(t - t_M) + A_C \cdot H(t - t_A)$$

where,

- d : Positional data from GPS time series.
- C_0 : Constant offset
- M_C : Coseismic displacement caused by the mainshock at time t_M
- M_P : Amplitude modulating the post-seismic relaxation of the mainshock
- A_C : Coseismic displacement caused by the M 7.9 aftershock at time t_A
- $H(*)$: Heaviside function.

We perform a weighted least squares fit, solving for d_0, M_C, M_P and A_C, with relative weights obtained from the formal errors on the observables. The formal errors, σ, are rescaled as follows:

$$\sigma^* = \frac{\sigma}{\bar{\sigma}} \cdot \mathrm{RMS}(d_{obs} - d_{fit})$$

where d_{obs} and d_{fit} are the observed and predicted data values. We removed a three-sample window centered at the closest sample to the mainshock and aftershock since these are consistently observed to be outliers in the positional time series.

Preparation and Modeling of Tsunami Records

The distribution of slip as a function of depth along the fault, in particular the extent of slip found near the trench, is most strongly constrained by incorporating the tsunami waveform data. We use deep sea-bottom pressure sensor records retrieved from the NOAA website (http://www.ndbc.noaa.gov/dart/dart.shtml)(*38*). We remove the ocean tidal signal using a polynomial filter. Because in deep water the amplitude of the tsunami wave is relatively small compared to the water depth, nonlinear propagation effects are negligible. Thus, we assume that the first oscillations of the tsunami signal are linearly related to the source (seafloor displacements) and that we can adopt a linear Green's function approach. The tsunami Green's functions are estimated based on the linear shallow water approximation using the Cornell Multi-Grid Coupled Tsunami Model code (http://ceeserver.cee.cornell.edu/pll-group/comcot.htm). The bathymetry is extracted from the ETOPO2 bathymetry grid, with a resolution of 2 arcminutes (*39*).

Seafloor displacements are in turn related to slip on individual triangular subfault patches through elastic Green's functions. The Green's function for each triangular patch is calculated by summing the contributions from a set of appropriately spaced and weighted point sources. For the purpose of modeling the tsunami wave heights, we treat slip during the earthquake as if it occurred simultaneously over the entire rupture. This approximation is valid because the earthquake rupture velocity is large compared to the tsunami propagation time.

We use 80 minute long records sampled at 1 min. We initially assume a 2.5 cm error for the tsunami records, but as with the GPS data, this error is inflated by a factor of 4 to account for systematic errors. After several tests, we found that we could not reconcile the timing of the first tsunami arrivals at four DART sensors closest to Japan with those observed at the distant stations offshore Alaska and Western USA. However, the waveforms at all 12 stations are well explained. Thus, we interpret these timing issues to be propagation effects from systematic errors in the bathymetry or the fact that dispersion has not been taken into account. Thus, in our inversions, we kept the records from the four nearest stations in absolute time, but allowed a time shift for the remaining 8 records. The applied time shift increases with propagation distance. With this time shift, we are able to fit all 12 full waveforms well.

Fault Geometry

We construct a model of the surface of the subducted Pacific Plate using the GOCAD® commercial software package. Using interpretations of seismic reflection and refraction profiles, the plate interface is constrained to depths of about 30 km. The deeper slab geometry is constrained with published seismic tomographic and earthquake hypocenters. We interpolate a smooth interface between the seismic lines, and allow a misfit between the interface model and the seismic profiles up to a kilometer in depth in places where the seismic profiles conflict as to the depth to the top of the Pacific plate. The trench location is estimated from bathymetric features as well as from trench locations in the seismic profiles. For modeling purposes, we tessellate the fault geometry using triangular patches that conform to the complex 3-D geometry of the megathrust. We use a total of 419 triangular patches with a characteristic dimension that ranges between 11 and 27 km.

Static Finite Fault Modeling

For modeling the static slip distribution for the mainshock rupture, we adopt a Bayesian approach because it has several advantages over traditional inversion methodologies. Determining slip on a fault based on surface observations is, in general, an under-determined inverse problem, and this under-determinedness is only exacerbated when trying to constrain off-shore slip with mainly land-based observations. Because of this ill-posedness, slip inversions have historically used *a priori* constraints on the solution such as Laplacian smoothing and moment minimization. Since the inverse problem has no unique solution, any slip model produced in this manner is only one sample from a conceivably large space of possible models. Such a slip model is predestined to conform to some *a priori* regularization, which may have been chosen without any physical basis.

In contrast, Bayesian analysis casts the solution to the inverse problem as an *a posteriori* probability density function (PDF), *P(M|D)*, the probability of a model *M* given observed data *D*, which is proportional to *P(M)·P(D|M)*, the product of the *a priori* probability of the model and the likelihood of the data. There are two main advantages to this approach. First, the inverse problem need never be evaluated because the *a posteriori* PDF can be determined through Monte Carlo simulation, and thus *a priori* regularization is not required to make the problem computationally stable. Second, computing the *a posteriori* PDF yields not one solution to the under-determined inverse problem, but instead returns the ensemble of all possible source models that are consistent with the data and our *a priori* assumptions about the physics of the earthquake source.

Our model for the earthquake rupture consists of two perpendicular components of slip on each cell of a complex triangulated mesh. We evaluate the data likelihood by calculating an L2 norm misfit function, $\mathrm{P(D|M)} = \mathrm{e}^{-\frac{1}{2}(\mathrm{D-G\cdot M})^{\mathrm{T}}\mathrm{C_D^{-1}}(\mathrm{D-G\cdot M})}$, where G is a matrix of Green's functions, $\mathrm{C_D}$ is the data covariance matrix, and M is the vector of slips on each patch. The Green's functions are calculated using a 1-D velocity model modified from (40).

Our goal is to determine what parts of the rupture process are well constrained by the data and which are not. To this end, we use broad *a priori* PDFs to describe our model so that the *a posteriori* distribution is controlled by the data likelihood. The strike-slip component of slip is assigned a Gaussian *a priori* probability with zero mean and a standard deviation of 10 m, while the dip-slip component is given a uniform probability between -10 m and infinity. (Negative slip denotes back-slip or normal faulting.) Drawing samples of the *a posteriori* PDF is extremely costly for inverse problems with large numbers of free parameters. To make the sampling process computationally tractable we use the Cascading Adaptive Transitional Metropolis In Parallel (CATMIP) algorithm (*6, 41*) which combines an adaptive implementation of the Metropolis algorithm, resampling and simulated annealing in a parallel framework. We list the coordinates for each triangular patch and the estimates of slip for each patch in Tables 1 and 2. The ID number for each triangle is shown in Fig. S12.

Since the Bayesian approach applies no smoothing to the model, this leads to the question: to what extent are the details of the slip distribution to be believed? The answer to this question comes in two forms. The first is to look at the correlation between any two model parameters

(e.g., slip on neighboring patches) using the ensemble of all models that comprise the PDF. If the model is not resolved, we should find considerable anti-correlation between neighbors. As an example, we show the correlation between the dip-slip component of motion on the patch with the peak slip and all other patches (Fig. S11). Note that there is only slight anti-correlation with one neighbor, so the slip distribution appears to be well constrained. A second answer to the resolution question comes in terms of understanding the output of the Bayesian sampling process. Our solution for fault slip is not a single model, but rather represents derived statistical quantities (specifically, the mean or median) from the PDFs for each model parameter. If there are trade-offs between fault patches, the mean should not be affected, but the variance about the mean will increase.

The above discussion on resolution is only strictly true in the context of a perfect physical model, but no model can be perfect. Furthermore, the uncertainty in the present physical model is not considered as part of the observation error (i.e., the data covariance matrix) that goes into evaluating the data likelihood, and thus the *a priori* observation error and the *a posteriori* model uncertainties underestimate the true error. The model design used in this study ignores the effects of topography, simplifies the elastic structure of the Earth and the geometry of the fault, and assumes that the tsunami is caused by instantaneous and simultaneous slip on the fault. These limitations in the physical model can cause systematic biases that are not explored here. For instance, our current parameterization can only alter the timing of the tsunami waveforms by varying the location of slip. A more sophisticated model in which slip on the fault evolves as a function of time would cause time-dependent seafloor displacements. Such extra degrees of freedom would improve the fit to both the GPS and tsunami data while inevitably changing the *a posteriori* distribution of fault slip.

The Mw 7.9 Aftershock

For the Mw 7.9 aftershock, we adopted a small, tessellated rectangular fault patch with a position and fault orientation based on the GCMT mechanism. We also constrained the magnitude (Mw 7.9) to be consistent with the CMT mechanism. The distribution of fault slip for this event was calculated using a simulated annealing approach (*42*).

Kinematic Finite Fault Modeling

The assumed fault plane extends 280 km down-dip and 500 km along-strike. The fault is tessellated with a grid of 20 km × 25 km-sized patches. The slip rake on each patch is constrained to ±90°, with slip triggered by the rupture front. We constrain the total moment to the value given by the GCMT best double-couple moment. The rupture velocity is allowed to vary between 0.9 and 2.0 km/s. We adopt a 1-D layered velocity model extracted from CRUST2.0 (*43*). We considered both a two fault plane model and a single fault plane model. The two models show similar fits to the GPS and teleseismic data.

High Frequency Seismic Wave Back Projection

We used P-wave seismograms recorded by two large arrays at epicentral distances of 70°-90°, the USArray and the European network, which illuminate the source region from two almost orthogonal directions (Fig. S8). We band-pass filtered the waveforms between 0.5 and 1 Hz and

aligned them on their first P arrival by multi-channel cross-correlation (*44*). We then applied two different array processing techniques over 10-second-long sliding windows, Multiple Signal Classification (MUSIC) (*14*, *45*) and coherent interferometry (CINT) (*15*, *46*) with back-projection onto the source region at a reference depth of 15 km with travel times based on the IASP91 Earth model. Our results based on MUSIC and CINT are mutually consistent. Compared to classical beam forming, these high-resolution techniques resolve more closely spaced sources and are less sensitive to aliasing, yielding a sharper and more robust image of the rupture process. The results from both arrays are consistent with each other.

We use the JMA hypocenter to fix the absolute location. Use of a different hypocenter would result in a simple translation of the radiator locations. Expected errors in the epicenter are sufficiently small that the conclusion about the location of the high frequency radiators relative to the distribution of fault slip is robust.

The back projection used USArray data available from http://www.usarray.org/ and http://www.iris.edu as well as from http://www.orfeus-eu.org and http://iside.rm.ingv.it.

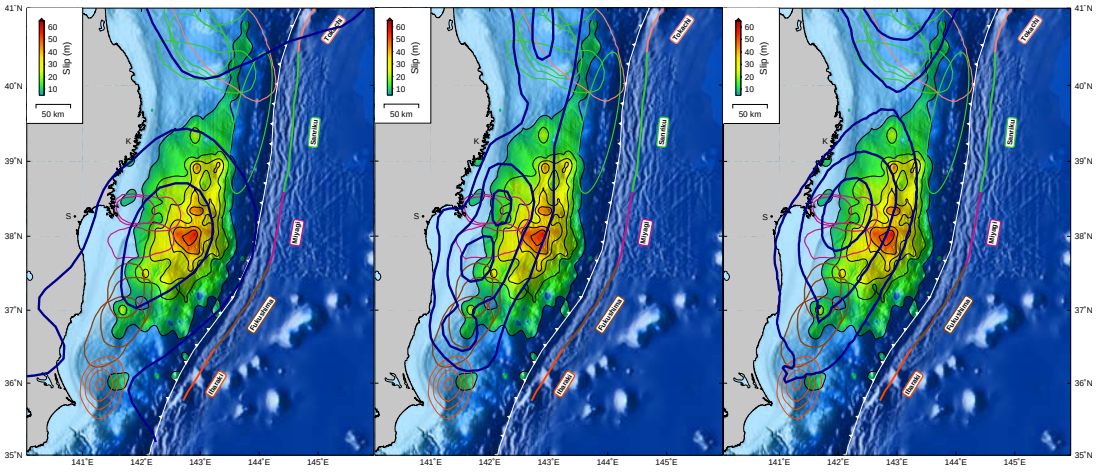

Fig. S1

Comparison of published fault coupling models (blue contours) constrained by GPS-based estimates of the secular interseismic surface velocity field. The contour intervals are equivalent to about (left) 50% and 95% coupling (*47*), (middle) 35%, 70% and 100% coupling (*3*), and (right) 30%, 60% and 90% coupling (*28*). Contours taken from original sources. Other features are as in Fig. 1. Differences between these models are mostly due to whether or not vertical deformation data is used, the amount of spatial smoothing that is applied, and the degree to which long term shortening on shallow on-land crustal faults is considered in each analysis.

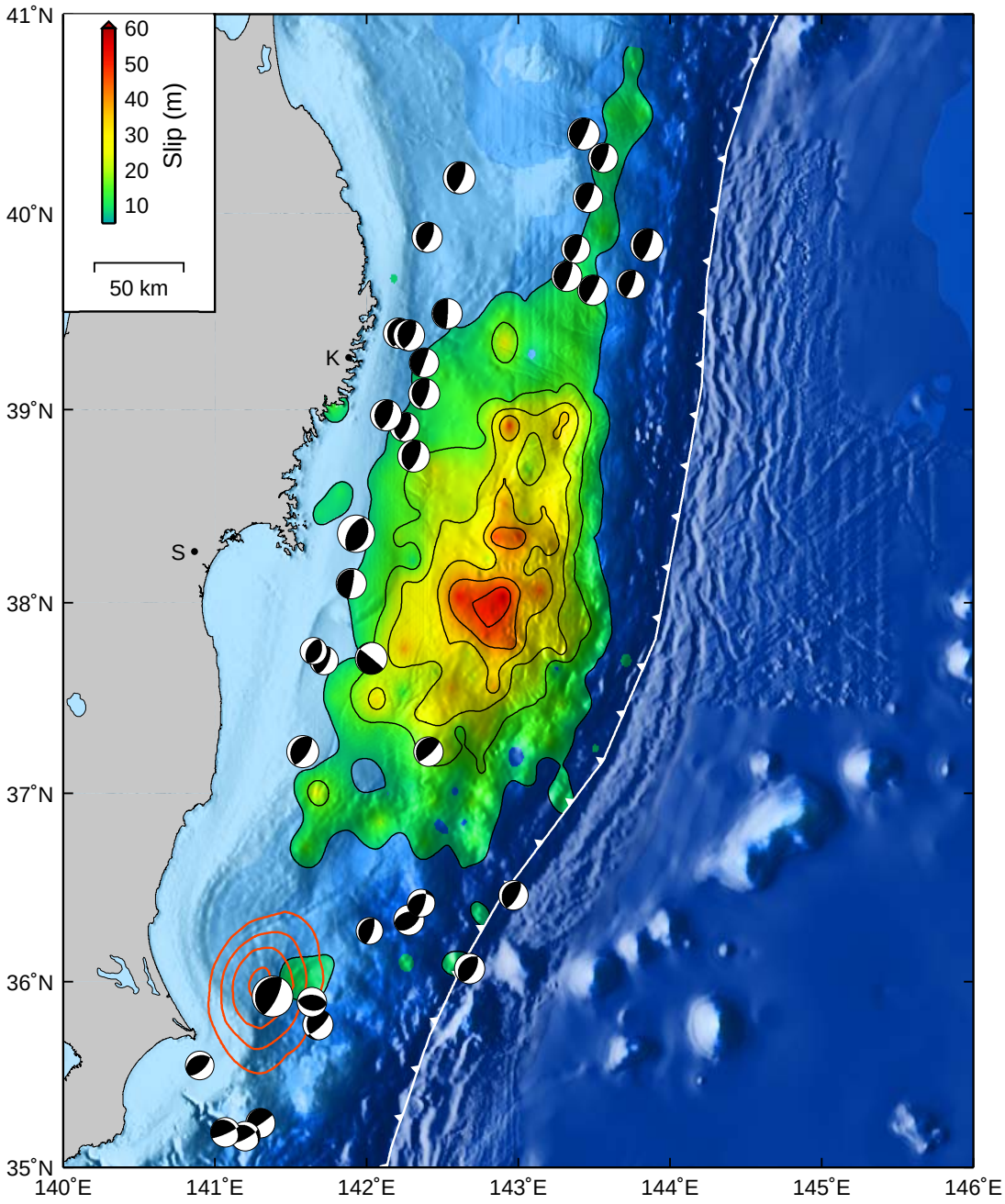

Fig. S2

Inferred distribution of subsurface fault slip (color with superimposed contours at 8 m intervals) constrained by GPS and tsunami observations and derived from an unregularized Bayesian estimation method (*6, 41*). The black focal mechanisms are GCMT solutions for a period of 34 days following the mainshock. Only events with thrust mechanisms are shown.

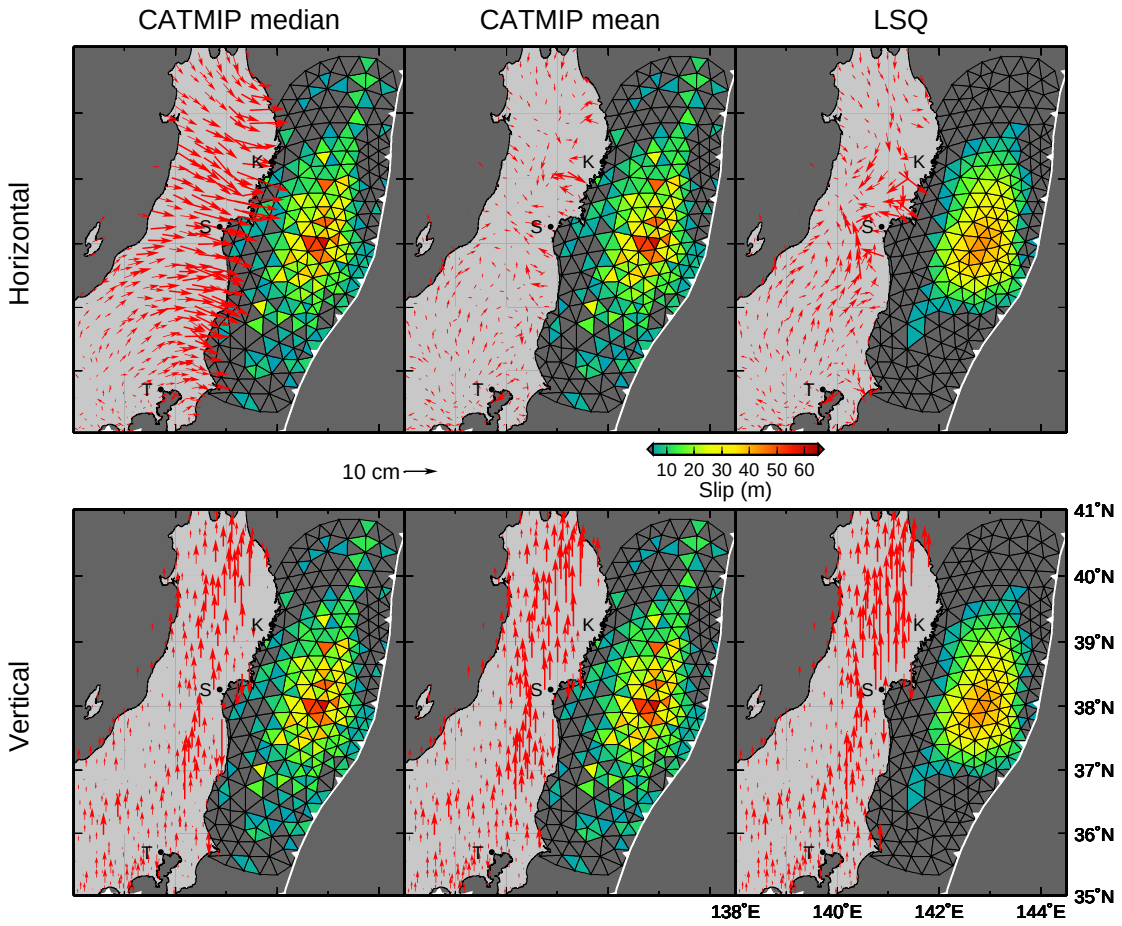

Fig. S3

Comparison of Bayesian slip models to results from conventional damped least squares (LSQ). The CATMIP median and CATMIP mean models are the median and mean, respectively, of the Bayesian *a posteriori* probability density function calculated using the CATMIP sampling algorithm. The LSQ approach simultaneously minimizes data misfit, spatial roughness of the slip model, and the difference between the inferred moment and a target moment equivalent to Mw 9.0. Red arrows show the residual horizontal (top) and vertical (bottom) GPS coseismic offsets. All three models fit the observed GPS data with a variance reduction of about 99%. The median and mean of the Bayesian *a posteriori* distribution are nearly identical and have almost equal overall goodness of fit to both the GPS and tsunami data, but these two slip models differ in a low amplitude, long wavelength spatial mode. This small difference causes a trade-off in how well they fit the horizontal component of the GPS displacements relative to the vertical component. This trade-off may be due to limitations in our assumed Earth structure and fault geometry.

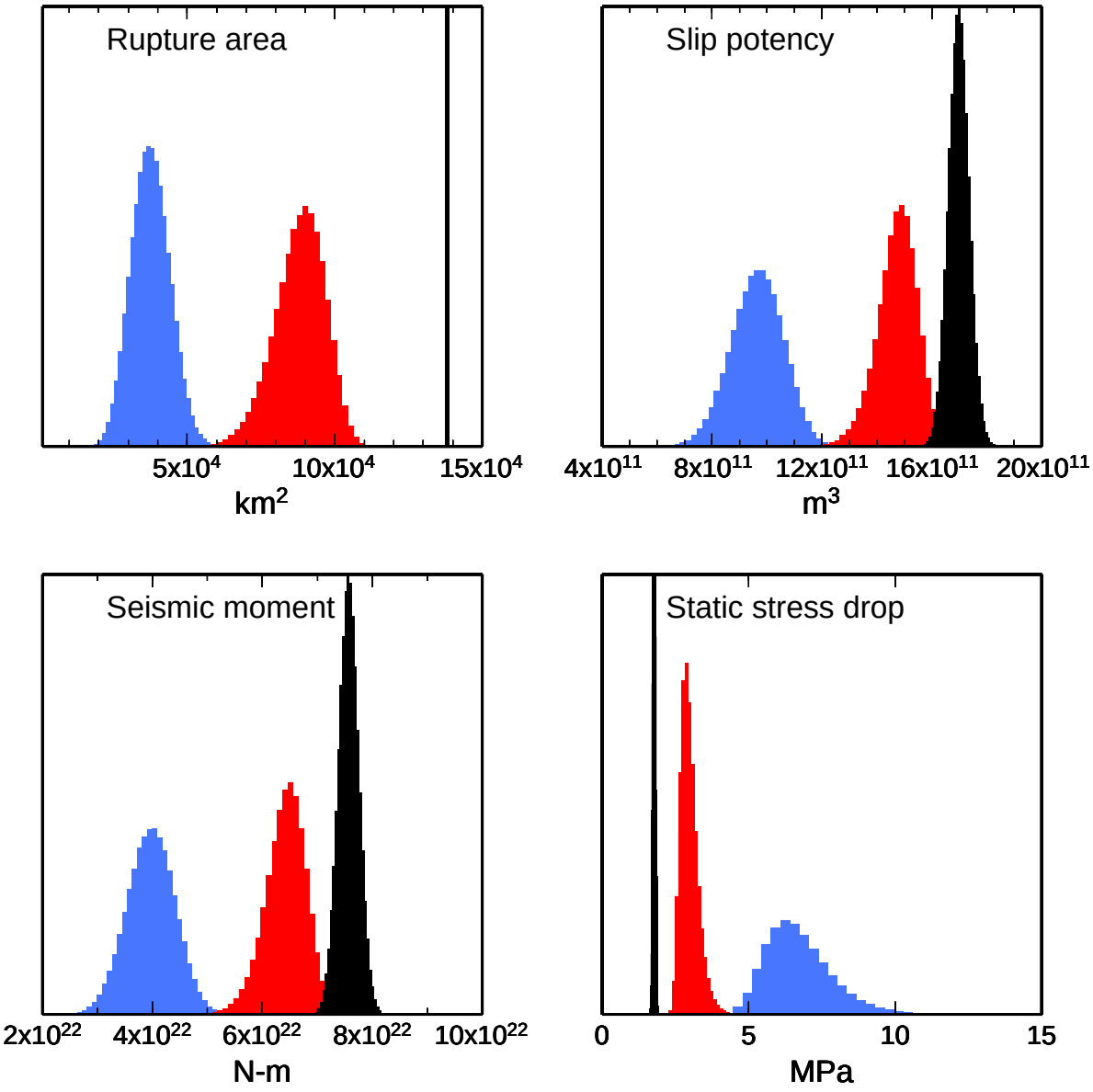

Fig. S4

A posteriori PDFs for derived quantities including rupture area, potency, scalar seismic moment and static stress drop. We consider three different thresholds to define the extent of the earthquake rupture: the entire fault model (black), areas that slipped in excess of 10% of the maximum slip (red), and in excess of 20% of the maximum slip (blue).

(A)

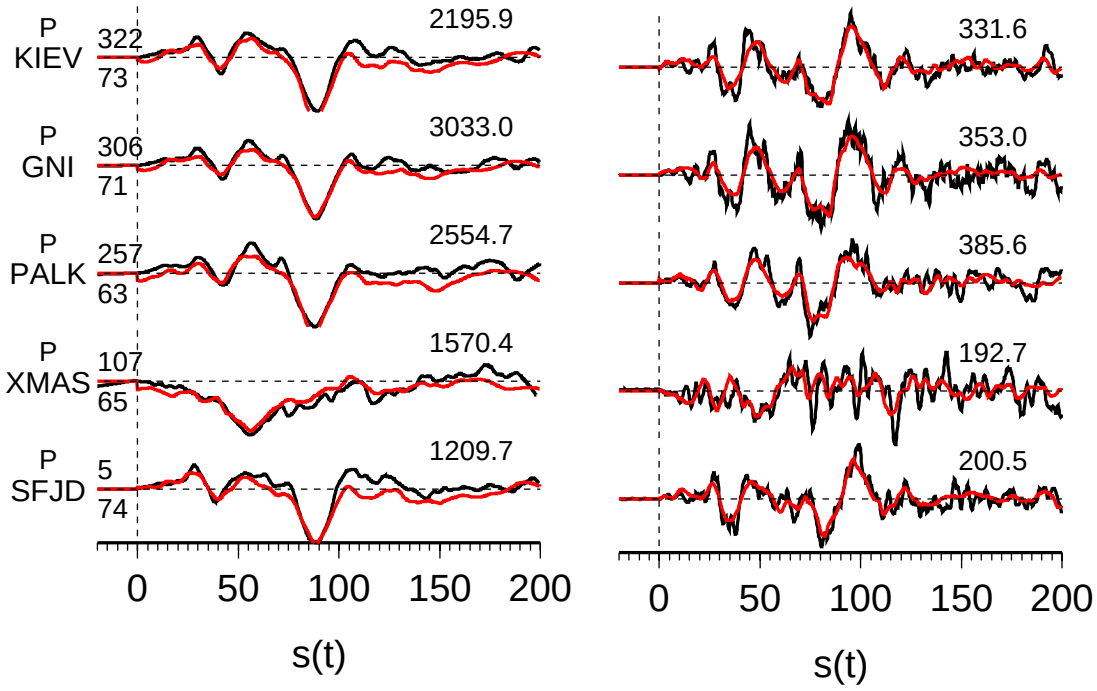

Fig. S5

(A) Sample waveform fits from the kinematic source model. Representative displacement (left column) and velocity (right column) waveform data (black) and fits (red) are shown. The number at the end of each trace is the peak amplitude of the observation in micro-meter or micro-meter per second. Station names are indicated to the left of the displacement seismogram with the numbers at the beginning of the trace indicating the source azimuth (top) and epicentral distance (bottom). Results from a larger sample (in velocity) are given in Fig. S5B for both the single and double plane solutions**.** **(B)** Comparison of an azimuthal sampling of P-waveforms against synthetics generated from the one-plane vs. two-plane solutions (see Fig. S6 for the corresponding slip models). The upper number indicates the azimuth with the lower number the distance in degrees. These two slip-models have been used to predict the waveforms globally. We consider the cross-correlations (cc) between data and synthetic waveforms (first 180s). Stations closer than 50 degrees contain the PP-wave in this time window, which lowers the fits. For example, see the recording at MAKZ near 150 s. Both the one and two plane models produce cc > .85 at over a 150 stations at ranges greater than 60 degrees.

(B)

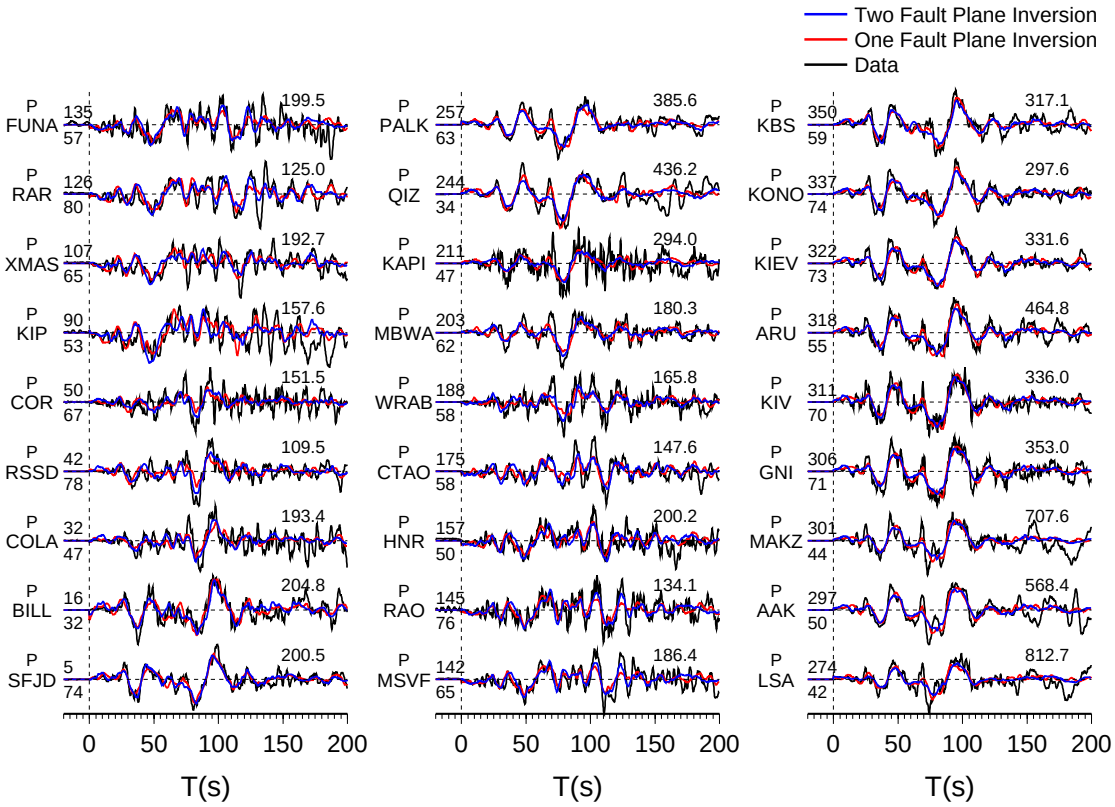

Fig. S5 continued

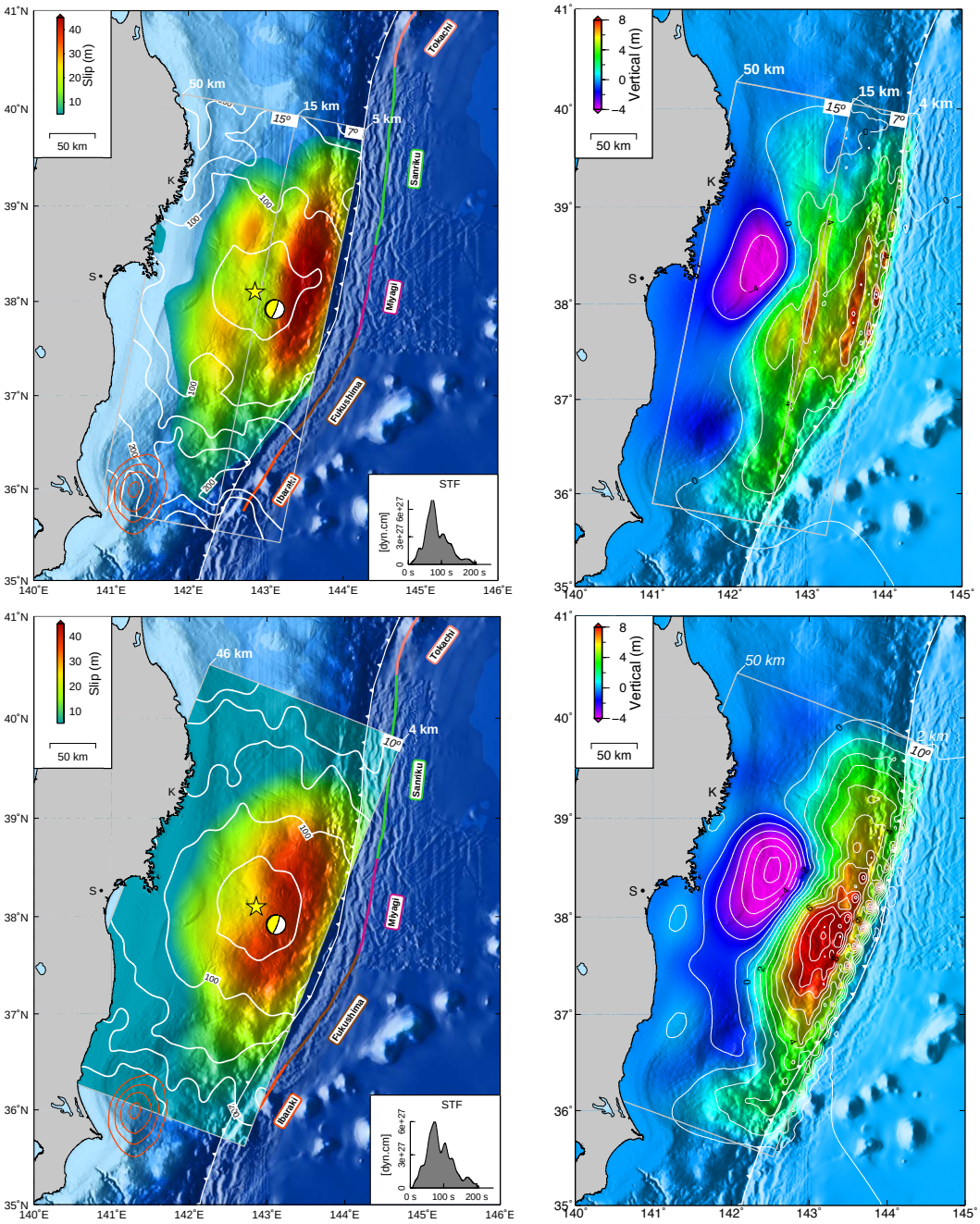

Fig. S6

Kinematic fault slip models constrained by GPS measurements and teleseismic P-waveforms. Estimated fault slip (left) and predicted vertical seafloor displacements (right) are shown for the two-plane (top) and one-plane (bottom) kinematic models. Dip angles and depth are given in the northeast corner of each fault plane. White contours indicate temporal evolution of the rupture front, with time in seconds. The yellow star shows the epicenter used for each inversion. The respective moment rate functions are plotted in the insets.

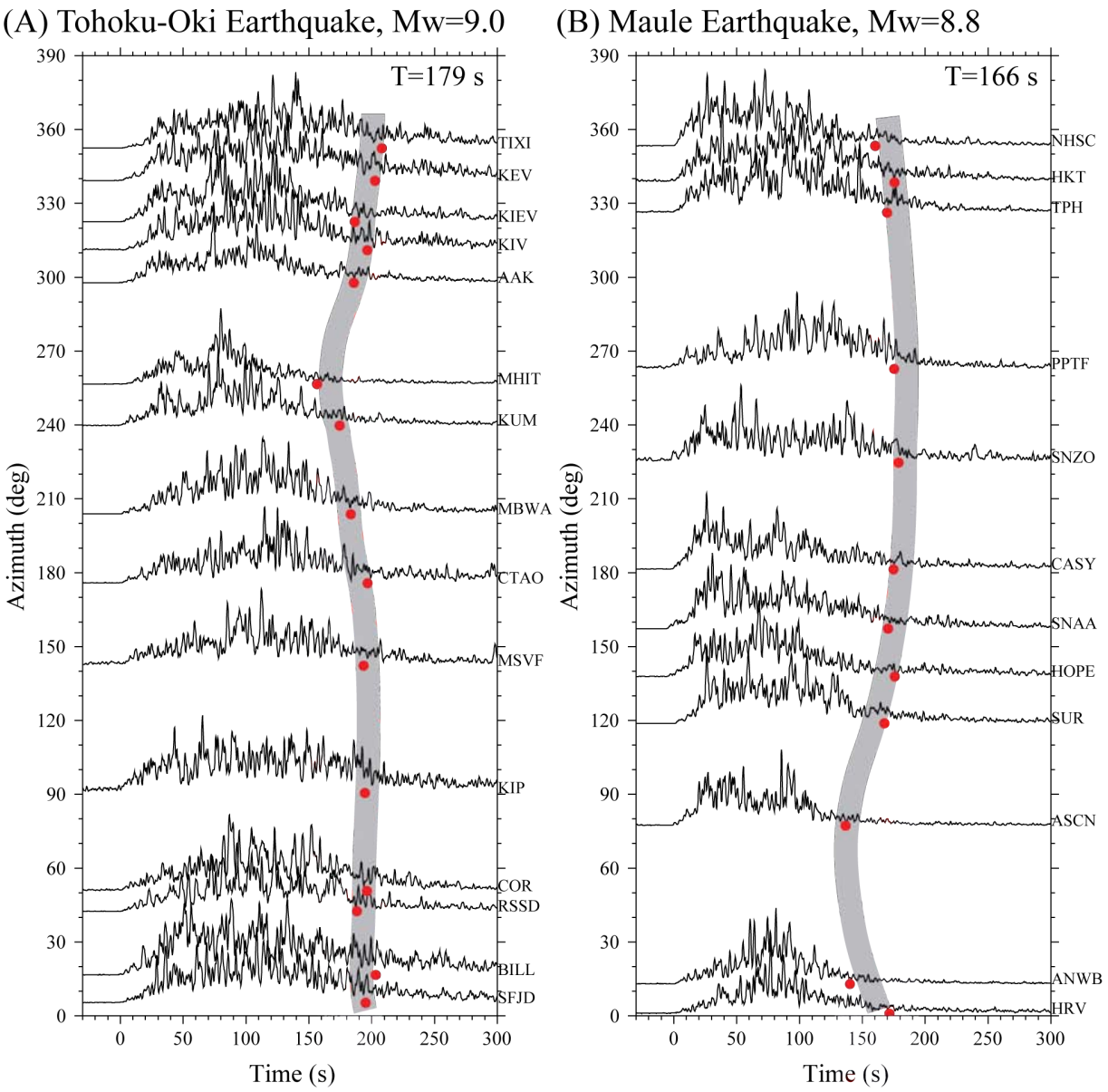

Fig. S7

Vertical component of smoothed teleseismic P-wave envelopes (band-passed at 2-4 Hz) for (A) the 2011 Tohoku-Oki earthquake and (B) the 2010 Maule earthquake as a function of azimuth. The envelopes are smoothed by convolving them with a triangle function of 2 s duration. Red dots represent the time by which 90% of the energy in the envelopes has been released. The slight relative decrease in this time at azimuths of 250 deg for the Tohoku event and 80 deg for the Maule event is caused by directivity.

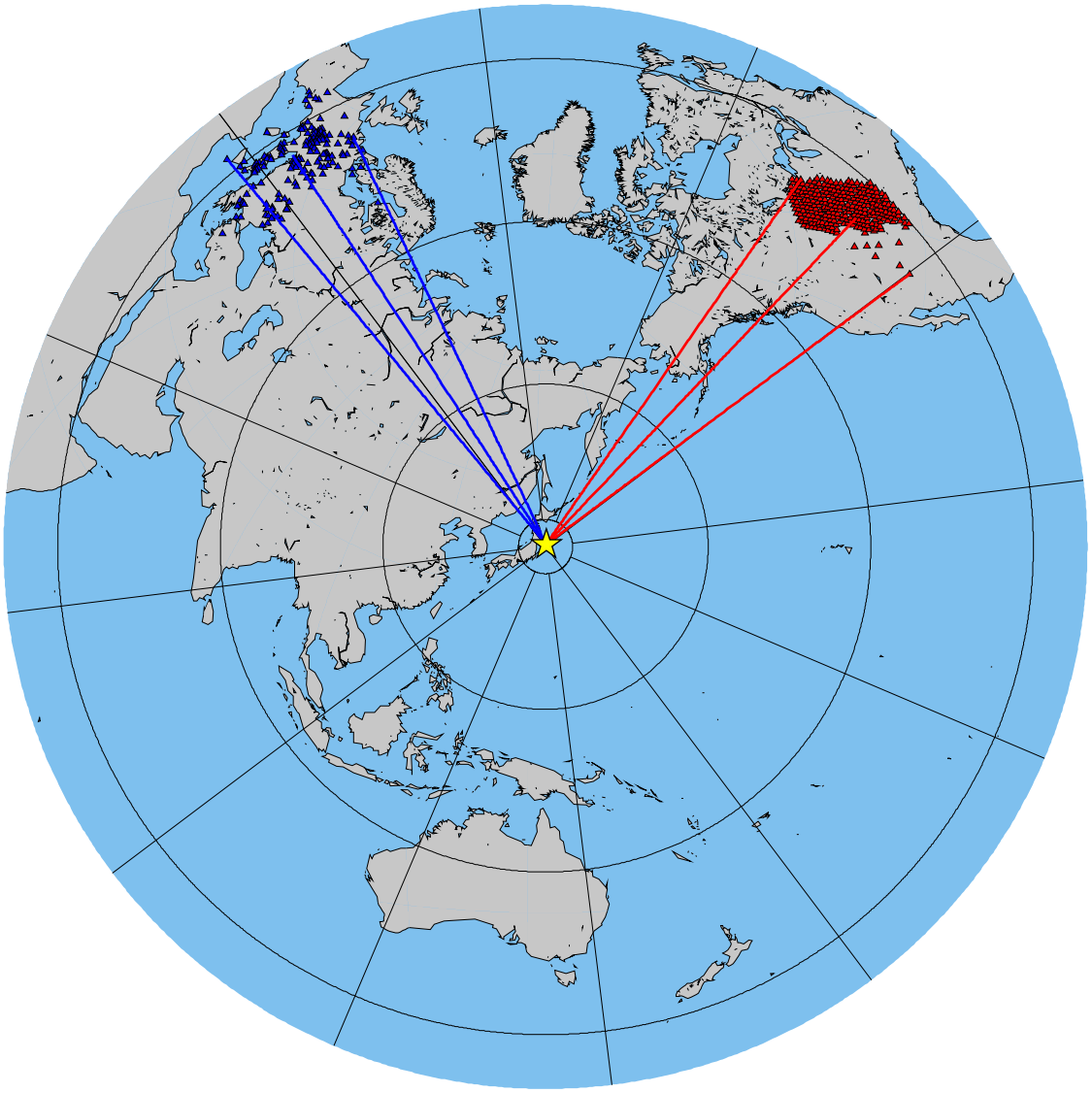

Fig. S8

Azimuthal equidistant projection centered on the 2011 Tohoku-Oki earthquake epicenter showing the approximate ray paths to the European seismic array (blue) and USarray (red). Concentric circles indicate distance from the epicenter at 30° intervals.

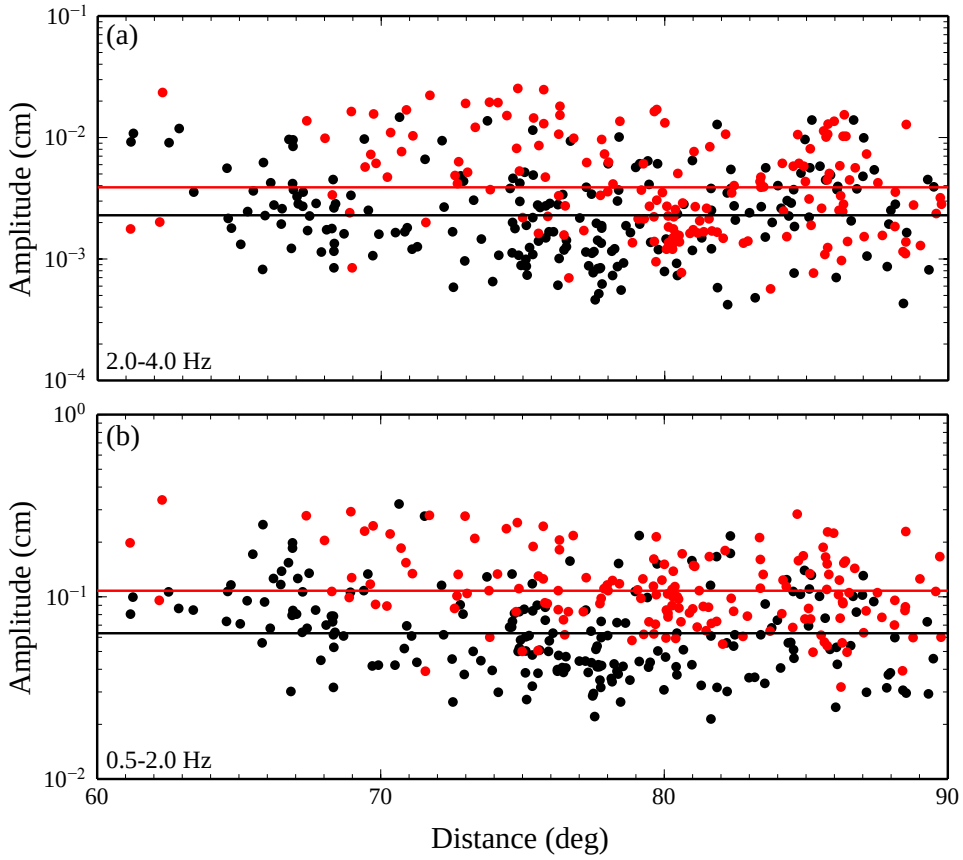

Fig. S9

Amplitude of the integrated teleseismic P-wave envelopes derived from the vertical component of seismograms in the (a) 2.0 to 4.0 Hz and (b) 0.5 to 2.0 Hz frequency bands, plotted as a function of distance from the centroid. Estimates for the 2011 Tohoku-Oki earthquake are indicated by black dots and estimates for the 2010 Maule with red dots. Black and red horizontal lines indicate the average of the log of the amplitude for each earthquake. Both the average and individual estimates for the Tohoku-Oki earthquake have been corrected for the difference in moment by a factor of $A/(10^{1.5\Delta M_w})$, where A is observed amplitude and ΔM_w denotes the magnitude difference between the two earthquakes.

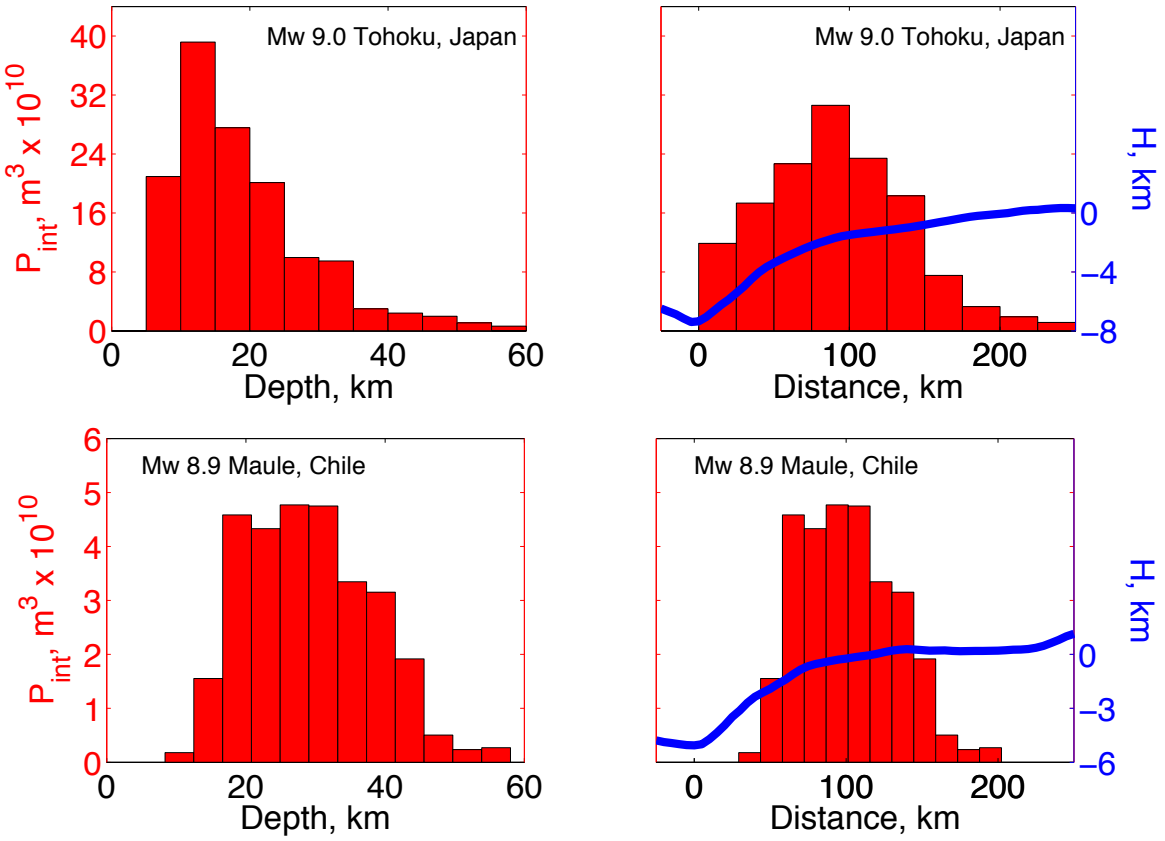

Fig. S10

Along-strike integrated potency (fault slip multiplied by area) as a function of depth (left) and distance from the trench (right). Also shown is the average bathymetric profile, *H*, versus distance from the trench (blue lines). Top row: 2011 Mw 9.0 Tohoku, Japan. Bottom row: 2010 Mw 8.8 Maule, Chile.

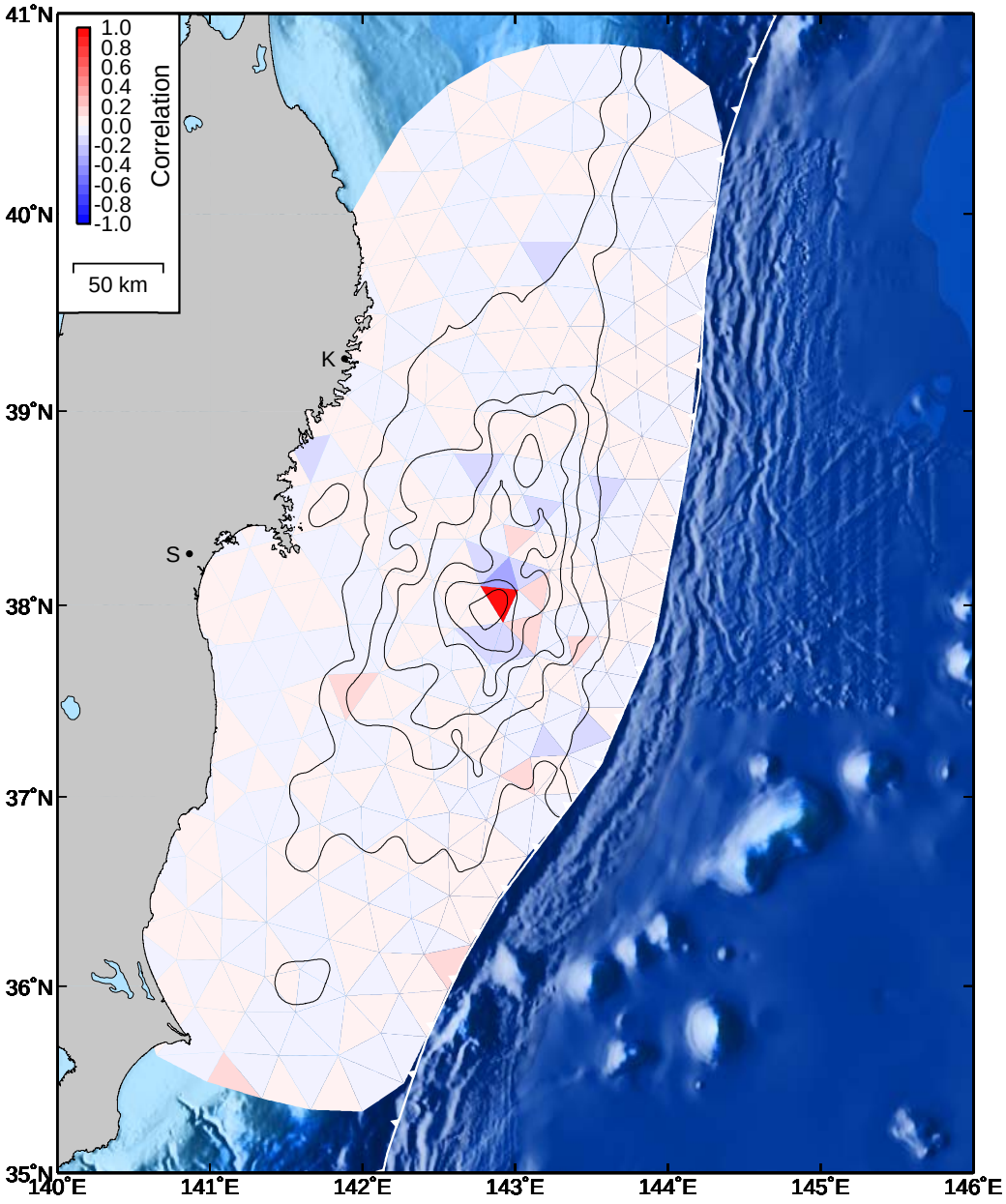

Fig. S11

Correlation of the up-dip component of slip on the fault patch with maximum average slip with the dip-slip component of slip on all other patches. These values are calculated from the Bayesian *a posteriori* PDF.

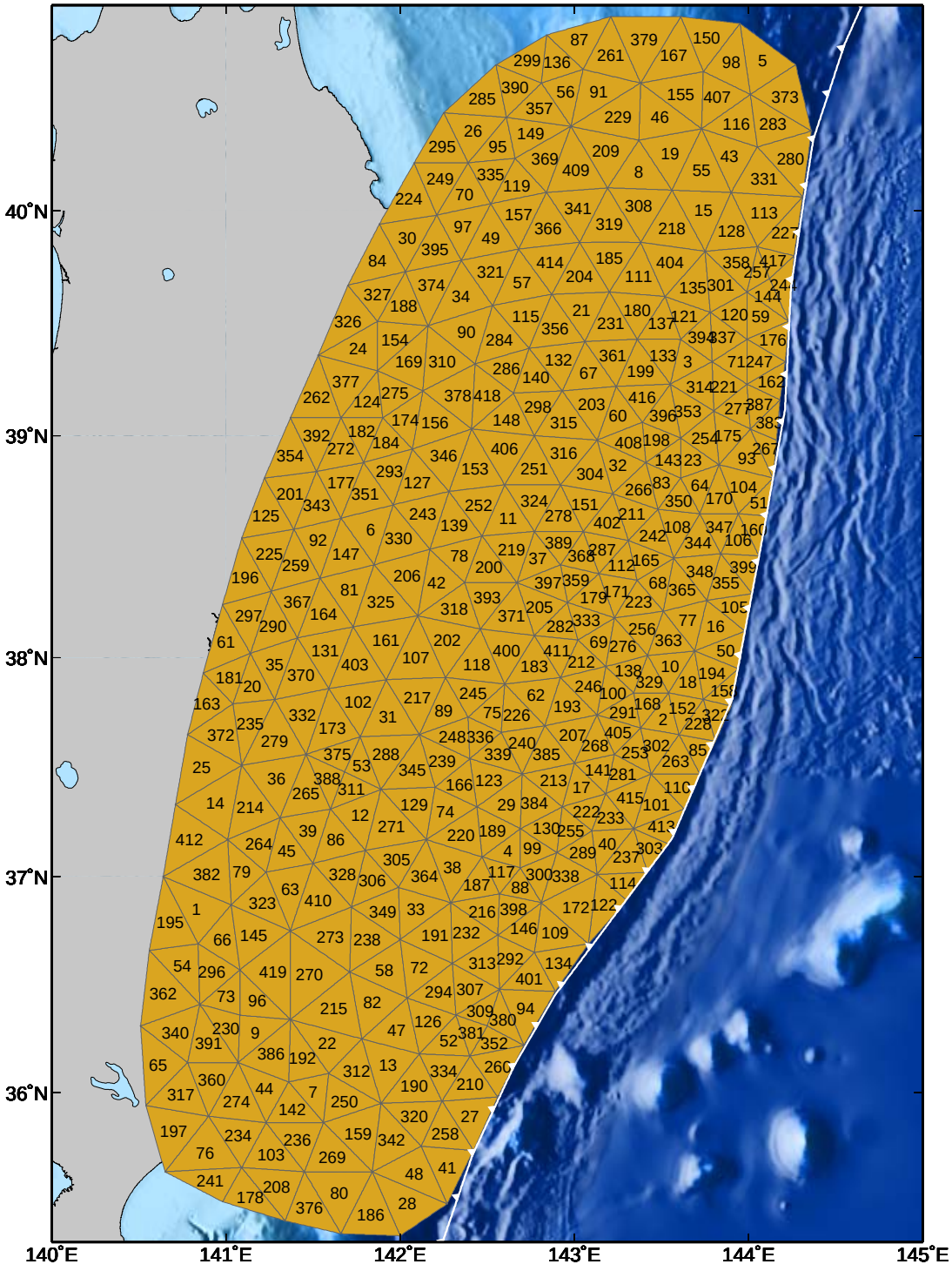

Fig. S12

Reference ID of each triangular patch used in the fault model. The geometry and estimated values of slip for each patch are given in Tables 1 and 2.

Table S1. Fault geometry.

Table S2. Fault slip.

Fault Geometry

Patch ID	Latitude	Longitude	Depth (km)	Strike	Dip	Area (km*km)
1	36.85	140.83	57.52	213	26	507.88
2	37.72	143.51	9.40	198	5	183.55
3	39.33	143.65	11.52	189	6	214.04
4	37.12	142.62	13.98	209	8	195.21
5	40.66	144.08	10.15	196	6	413.77
6	38.58	141.83	45.73	190	23	385.61
7	36.00	141.50	23.70	199	18	272.47
8	40.17	143.37	16.70	191	11	365.32
9	36.28	141.17	36.35	199	21	336.92
10	37.96	143.55	9.73	195	5	238.99
11	38.63	142.62	23.45	188	13	327.88
12	37.28	141.77	32.82	204	23	389.73
13	36.13	141.93	15.01	201	11	475.53
14	37.34	140.94	65.43	202	25	642.25
15	40.00	143.74	11.46	194	7	446.16
16	38.14	143.81	8.28	183	3	296.59
17	37.41	143.04	11.65	208	7	230.09
18	37.89	143.65	8.86	192	4	207.03
19	40.25	143.55	14.54	198	9	409.94
20	37.87	141.15	65.10	194	26	298.31
21	39.56	143.04	19.87	192	11	340.47
22	36.23	141.58	23.75	197	18	455.80
23	38.89	143.68	10.01	200	5	193.98
24	39.39	141.76	53.05	191	27	406.18
25	37.50	140.86	71.62	204	26	604.69
26	40.35	142.42	40.14	195	20	370.68
27	35.89	142.40	7.81	206	8	395.50
28	35.48	142.04	9.27	210	8	531.60
29	37.33	142.61	15.99	205	10	315.44
30	39.88	142.04	47.83	197	24	406.61
31	37.73	141.93	34.08	197	19	458.44
32	38.87	143.25	14.06	199	8	293.35
33	36.85	142.09	18.13	216	12	354.71
34	39.62	142.35	34.93	196	18	455.21
35	37.97	141.28	61.03	193	26	364.13
36	37.45	141.29	53.60	199	26	535.81
37	38.45	142.79	19.40	188	11	243.25

38	37.04	142.30	17.37	214	11	411.59
39	37.21	141.47	42.39	203	26	386.28
40	37.15	143.19	8.96	212	5	229.25
41	35.65	142.27	7.69	207	7	385.52
42	38.34	142.21	31.71	191	17	362.34
43	40.24	143.89	10.81	197	7	367.12
44	36.02	141.22	32.32	195	19	355.08
45	37.12	141.35	45.21	205	26	342.60
46	40.41	143.49	16.12	194	9	434.77
47	36.29	141.98	15.01	186	11	406.64
48	35.62	142.08	9.69	198	8	480.08
49	39.88	142.52	33.03	195	17	369.42
50	38.03	143.87	7.89	189	4	219.81
51	38.70	144.06	7.18	189	3	133.98
52	36.24	142.28	10.97	193	6	264.44
53	37.51	141.78	35.76	198	21	225.67
54	36.59	140.75	54.08	203	20	419.15
55	40.18	143.73	12.15	195	7	452.23
56	40.52	142.95	27.02	193	17	265.14
57	39.68	142.70	27.00	196	14	385.01
58	36.57	141.91	18.32	201	15	439.53
59	39.53	144.07	8.06	184	4	243.19
60	39.09	143.25	15.05	197	8	261.96
61	38.07	141.00	74.48	193	28	411.21
62	37.83	142.78	17.15	199	10	322.88
63	36.94	141.37	40.93	203	25	411.19
64	38.78	143.72	9.38	194	5	197.95
65	36.13	140.61	52.15	191	19	494.29
66	36.71	140.98	49.19	210	20	343.01
67	39.28	143.08	18.14	196	9	313.49
68	38.34	143.48	10.67	184	6	221.58
69	38.07	143.14	13.59	190	8	207.17
70	40.07	142.37	38.95	193	20	312.60
71	39.33	143.93	8.99	183	6	189.63
72	36.58	142.11	14.93	217	10	383.98
73	36.45	141.00	44.15	205	20	256.66
74	37.30	142.26	20.95	212	13	320.05
75	37.75	142.53	20.71	198	12	214.05
76	35.72	140.88	40.72	189	19	587.08
77	38.17	143.65	9.25	185	5	267.78
78	38.46	142.34	29.16	191	17	292.41
79	37.02	141.09	52.61	213	25	354.46
80	35.53	141.65	16.88	193	16	585.50
81	38.31	141.71	47.76	194	24	426.96

82	36.42	141.84	18.53	199	15	468.55
83	38.79	143.50	11.23	196	6	179.22
84	39.78	141.87	52.96	193	25	422.35
85	37.58	143.71	7.78	208	4	173.17
86	37.17	141.63	35.32	204	23	382.22
87	40.75	143.03	26.63	194	17	352.44
88	36.95	142.69	11.97	209	7	172.61
89	37.76	142.25	26.05	199	14	311.79
90	39.46	142.38	32.76	196	18	442.73
91	40.52	143.14	22.89	193	14	416.99
92	38.53	141.53	56.45	192	25	364.60
93	38.90	143.99	7.87	189	4	293.67
94	36.39	142.72	8.20	220	5	397.42
95	40.28	142.56	35.47	192	19	245.76
96	36.43	141.18	38.30	203	21	314.40
97	39.93	142.36	37.91	198	20	341.85
98	40.65	143.90	11.73	192	7	364.38
99	37.13	142.76	12.51	213	8	184.49
100	37.84	143.22	12.16	197	6	195.34
101	37.33	143.47	8.13	212	4	306.25
102	37.80	141.76	40.43	199	22	422.09
103	35.71	141.26	29.00	189	19	408.94
104	38.77	143.97	7.80	195	4	291.06
105	38.23	143.92	7.74	184	3	207.42
106	38.53	143.94	7.66	182	3	193.57
107	38.00	142.09	32.41	194	17	500.12
108	38.59	143.59	10.03	189	5	255.10
109	36.74	142.89	9.19	209	5	349.05
110	37.41	143.59	7.79	210	4	219.37
111	39.71	143.37	15.39	180	9	346.74
112	38.42	143.27	12.79	183	7	180.39
113	39.99	144.09	8.60	198	5	442.08
114	36.97	143.28	7.71	214	4	179.97
115	39.53	142.72	25.50	197	14	356.79
116	40.38	143.93	10.86	186	7	338.53
117	37.02	142.58	13.64	211	8	160.91
118	37.97	142.44	23.90	192	13	404.76
119	40.11	142.67	30.98	193	17	283.85
120	39.54	143.92	9.19	183	6	212.42
121	39.53	143.63	11.95	185	7	208.97
122	36.87	143.17	7.83	213	4	294.32
123	37.44	142.51	18.33	209	11	319.36
124	39.15	141.81	49.08	185	24	252.41
125	38.64	141.23	70.14	191	27	412.30

126	36.33	142.16	12.49	198	7	338.29
127	38.79	142.10	37.63	186	19	370.34
128	39.91	143.90	9.77	192	5	358.81
129	37.33	142.08	25.07	206	17	380.07
130	37.22	142.84	12.36	208	8	230.92
131	38.03	141.57	49.66	196	25	434.34
132	39.34	142.91	20.84	198	11	317.36
133	39.36	143.51	13.14	189	8	237.28
134	36.60	142.91	8.28	213	5	314.97
135	39.66	143.68	11.49	180	7	327.77
136	40.65	142.90	29.16	194	17	236.05
137	39.50	143.50	13.47	182	8	222.06
138	37.94	143.31	11.59	195	6	173.34
139	38.60	142.31	30.72	188	17	366.80
140	39.26	142.78	22.66	192	12	268.26
141	37.49	143.14	11.20	206	7	188.97
142	35.92	141.38	26.51	195	19	333.11
143	38.89	143.54	11.21	197	6	176.79
144	39.62	144.11	7.80	181	4	155.89
145	36.73	141.16	43.94	204	23	506.99
146	36.76	142.71	10.54	207	6	261.65
147	38.47	141.69	50.04	191	23	404.56
148	39.07	142.61	25.15	184	14	327.24
149	40.34	142.75	30.64	195	17	321.50
150	40.76	143.76	13.64	197	8	364.01
151	38.69	143.06	15.84	191	9	270.43
152	37.77	143.62	8.76	200	4	173.97
153	38.85	142.43	28.62	185	16	433.50
154	39.43	141.97	45.09	193	23	334.65
155	40.51	143.61	14.76	186	10	424.57
156	39.06	142.20	35.48	184	18	414.81
157	39.98	142.68	29.76	196	17	356.42
158	37.85	143.86	7.66	193	3	139.71
159	35.81	141.76	15.84	199	14	538.61
160	38.58	144.03	7.24	182	3	133.98
161	38.08	141.92	38.42	196	21	521.30
162	39.24	144.13	7.48	184	4	169.29
163	37.79	140.89	75.29	198	27	344.23
164	38.20	141.56	52.15	193	24	429.32
165	38.44	143.41	11.38	186	6	213.83
166	37.42	142.34	20.90	203	13	251.67
167	40.68	143.57	15.81	190	10	433.04
168	37.79	143.42	10.23	200	5	157.31
169	39.33	142.05	41.22	189	22	405.85

170	38.72	143.83	8.53	192	4	228.79
171	38.30	143.24	12.92	186	7	204.23
172	36.86	143.01	8.87	207	5	477.77
173	37.68	141.61	44.40	195	23	433.89
174	39.07	142.03	40.83	185	22	271.47
175	39.00	143.88	8.77	196	5	234.58
176	39.43	144.14	7.51	185	4	191.73
177	38.79	141.66	53.42	188	25	326.11
178	35.51	141.14	32.19	183	19	366.41
179	38.27	143.11	14.40	183	8	241.52
180	39.56	143.36	15.29	187	9	304.79
181	37.91	141.02	71.69	194	28	315.04
182	39.02	141.78	49.66	187	24	243.72
183	37.96	142.77	18.07	191	10	325.68
184	38.97	141.92	44.51	184	22	258.66
185	39.79	143.20	18.04	187	11	372.94
186	35.43	141.83	12.17	189	13	506.82
187	36.96	142.44	14.65	213	8	251.73
188	39.58	142.02	44.71	194	23	346.23
189	37.21	142.53	15.86	213	10	271.46
190	36.03	142.08	12.22	194	8	395.50
191	36.73	142.20	15.37	211	10	414.06
192	36.16	141.44	27.07	196	18	352.50
193	37.78	142.96	14.60	198	7	299.10
194	37.93	143.79	8.16	197	4	240.60
195	36.79	140.68	60.95	219	25	486.83
196	38.36	141.11	72.64	192	27	430.27
197	35.82	140.70	47.12	191	20	569.02
198	38.98	143.47	12.24	200	7	186.65
199	39.29	143.38	14.35	192	8	307.93
200	38.41	142.51	24.88	188	14	313.05
201	38.74	141.37	64.79	190	27	407.13
202	38.08	142.27	28.42	198	16	457.48
203	39.14	143.10	17.14	197	9	347.12
204	39.71	143.03	20.63	189	11	367.98
205	38.23	142.80	18.56	193	10	298.67
206	38.37	142.04	37.05	191	21	463.88
207	37.65	142.99	13.63	204	8	294.10
208	35.56	141.29	27.37	184	19	450.28
209	40.26	143.18	20.56	195	13	436.60
210	36.04	142.40	8.82	207	8	318.02
211	38.65	143.33	12.44	190	7	238.73
212	37.98	143.04	14.50	192	7	192.95
213	37.44	142.88	13.52	205	8	293.78

214	37.32	141.14	57.36	202	25	505.53
215	36.39	141.62	24.01	194	18	620.52
216	36.84	142.47	13.39	211	8	261.42
217	37.82	142.10	30.51	200	18	455.28
218	39.92	143.56	13.18	187	8	452.34
219	38.49	142.64	22.39	190	14	336.94
220	37.19	142.35	18.25	208	11	349.65
221	39.22	143.86	9.36	191	5	202.26
222	37.30	143.07	10.73	208	7	187.18
223	38.25	143.37	11.65	182	6	215.48
224	40.05	142.05	49.19	193	23	428.75
225	38.47	141.25	67.81	192	27	422.85
226	37.74	142.67	18.30	201	10	255.92
227	39.90	144.21	7.60	194	4	269.01
228	37.70	143.71	8.06	198	4	183.19
229	40.41	143.25	20.21	191	13	485.71
230	36.30	141.00	42.21	199	20	278.30
231	39.50	143.21	17.20	188	9	317.75
232	36.74	142.38	13.33	220	8	368.67
233	37.27	143.21	9.48	211	5	196.41
234	35.80	141.07	35.12	189	19	385.98
235	37.70	141.14	63.53	197	26	363.38
236	35.78	141.41	24.60	190	19	398.12
237	37.09	143.30	8.07	210	4	288.94
238	36.71	141.81	22.43	205	17	449.30
239	37.53	142.24	24.17	207	14	296.43
240	37.61	142.70	16.84	203	10	252.94
241	35.59	140.91	39.41	183	19	371.25
242	38.55	143.45	11.14	185	6	259.84
243	38.65	142.13	35.88	190	20	380.24
244	39.67	144.20	7.29	187	4	173.20
245	37.84	142.42	23.44	201	13	293.80
246	37.87	143.08	13.66	196	8	267.17
247	39.33	144.06	7.96	185	4	205.37
248	37.64	142.30	23.97	200	14	269.16
249	40.14	142.23	44.21	195	22	372.70
250	35.96	141.68	19.00	202	14	382.29
251	38.85	142.77	21.27	187	12	345.41
252	38.69	142.45	27.49	191	16	360.90
253	37.57	143.35	9.89	204	5	188.67
254	38.99	143.75	9.79	193	6	254.63
255	37.21	142.98	11.00	212	7	190.22
256	38.13	143.39	11.33	188	6	264.29
257	39.73	144.05	8.28	186	5	113.86

258	35.81	142.26	8.83	210	7	326.56
259	38.42	141.40	60.86	191	25	372.37
260	36.12	142.56	7.88	215	7	339.89
261	40.68	143.21	22.21	191	14	415.71
262	39.17	141.52	61.56	189	27	451.42
263	37.53	143.58	8.25	206	4	256.00
264	37.15	141.19	52.36	205	26	359.37
265	37.38	141.46	45.78	198	25	412.53
266	38.76	143.37	12.41	194	7	235.99
267	38.94	144.10	7.28	189	4	132.17
268	37.60	143.12	11.97	203	6	217.49
269	35.70	141.61	18.63	187	16	471.27
270	36.55	141.48	30.27	202	22	742.85
271	37.23	141.95	26.83	207	17	472.83
272	38.94	141.66	54.26	186	25	309.85
273	36.72	141.60	28.90	199	22	558.79
274	35.96	141.06	36.53	195	19	468.05
275	39.19	141.97	43.49	186	22	264.74
276	38.05	143.28	12.18	190	6	244.91
277	39.12	143.94	8.63	187	5	192.55
278	38.64	142.91	17.91	187	10	274.04
279	37.62	141.28	56.64	197	25	545.31
280	40.23	144.24	8.12	191	5	416.89
281	37.47	143.28	9.93	209	5	197.13
282	38.14	142.92	16.57	188	9	201.08
283	40.38	144.14	9.11	192	5	346.28
284	39.43	142.57	27.81	195	14	362.22
285	40.49	142.47	39.89	192	20	418.82
286	39.30	142.61	26.09	193	14	278.28
287	38.49	143.16	14.07	188	8	217.38
288	37.56	141.92	32.16	204	20	440.78
289	37.11	143.05	9.85	207	6	209.30
290	38.14	141.27	63.08	193	26	367.73
291	37.75	143.28	11.24	196	6	187.84
292	36.62	142.63	10.32	220	6	263.38
293	38.84	141.94	43.20	188	22	337.20
294	36.47	142.22	12.63	211	7	333.73
295	40.28	142.24	45.23	192	22	342.99
296	36.56	140.92	48.35	204	20	357.98
297	38.19	141.13	69.94	193	28	395.43
298	39.13	142.79	21.87	192	12	270.69
299	40.66	142.73	33.65	193	19	293.08
300	37.01	142.80	11.32	209	7	207.11
301	39.67	143.84	9.94	181	6	282.06

302	37.60	143.47	9.18	208	5	214.93
303	37.13	143.43	7.56	211	4	170.38
304	38.83	143.09	15.96	192	9	339.63
305	37.08	141.98	23.66	212	18	359.99
306	36.98	141.84	25.48	208	18	333.80
307	36.48	142.40	11.12	216	6	311.71
308	40.02	143.37	16.03	193	11	416.61
309	36.38	142.46	9.99	212	5	166.82
310	39.33	142.24	35.49	190	19	430.72
311	37.40	141.72	36.15	199	21	219.76
312	36.10	141.75	18.27	190	15	402.11
313	36.60	142.47	11.38	216	6	335.90
314	39.22	143.72	10.68	189	6	262.17
315	39.06	142.94	19.05	188	10	369.40
316	38.92	142.94	18.53	195	10	373.71
317	35.99	140.74	47.02	195	20	431.33
318	38.22	142.31	28.52	188	16	359.92
319	39.94	143.20	18.61	190	12	407.89
320	35.89	142.08	11.36	209	9	358.45
321	39.73	142.52	31.48	198	17	384.96
322	37.74	143.81	7.66	202	3	137.19
323	36.88	141.21	45.17	210	23	412.40
324	38.71	142.77	20.77	191	13	322.23
325	38.25	141.89	40.83	193	20	513.85
326	39.51	141.70	56.80	192	27	417.37
327	39.63	141.87	51.27	196	26	328.27
328	37.01	141.67	31.15	205	23	405.33
329	37.89	143.43	10.47	194	5	164.67
330	38.54	141.99	39.66	189	20	395.03
331	40.14	144.09	8.96	193	5	410.27
332	37.74	141.44	51.48	195	26	466.77
333	38.17	143.07	14.70	192	8	209.45
334	36.10	142.25	10.69	206	6	307.03
335	40.16	142.52	35.29	195	19	260.97
336	37.64	142.46	20.97	204	12	179.07
337	39.44	143.85	9.68	184	6	210.60
338	37.00	142.95	10.02	211	6	307.49
339	37.56	142.56	18.59	201	11	246.02
340	36.28	140.71	50.56	200	18	444.32
341	40.01	143.02	22.39	193	14	392.90
342	35.78	141.95	12.24	204	9	424.78
343	38.69	141.52	58.06	189	25	348.47
344	38.52	143.71	9.06	184	4	248.28
345	37.49	142.07	27.37	201	16	369.48

346	38.91	142.25	33.60	188	19	425.60
347	38.59	143.83	8.33	187	4	194.85
348	38.39	143.72	8.89	184	4	251.88
349	36.84	141.90	21.80	203	17	333.86
350	38.71	143.60	10.14	192	5	176.25
351	38.74	141.80	47.50	187	23	349.73
352	36.23	142.54	8.75	200	6	194.10
353	39.11	143.65	10.96	196	6	258.08
354	38.91	141.37	66.37	188	27	408.57
355	38.34	143.87	8.00	180	3	239.93
356	39.48	142.89	21.96	194	11	337.87
357	40.45	142.80	30.19	190	17	312.46
358	39.77	143.93	9.28	187	5	280.45
359	38.35	143.01	15.82	188	9	179.88
360	36.06	140.92	42.02	195	20	374.97
361	39.36	143.22	16.59	194	9	301.94
362	36.46	140.64	55.23	207	20	612.38
363	38.08	143.54	10.00	185	5	260.21
364	37.00	142.14	19.25	212	12	389.21
365	38.31	143.62	9.61	182	5	270.19
366	39.92	142.85	25.41	193	14	389.63
367	38.25	141.41	58.83	193	26	375.91
368	38.46	143.04	15.63	185	9	183.91
369	40.23	142.83	27.91	193	17	362.22
370	37.92	141.43	54.29	193	26	426.56
371	38.19	142.64	21.26	188	12	360.56
372	37.65	140.97	69.85	197	27	432.35
373	40.50	144.21	8.77	187	5	404.52
374	39.67	142.18	40.37	198	22	414.36
375	37.56	141.64	41.64	199	25	225.88
376	35.46	141.48	21.22	184	19	429.59
377	39.24	141.69	54.76	189	27	460.71
378	39.18	142.33	32.41	186	18	425.85
379	40.75	143.40	19.09	195	13	536.07
380	36.34	142.59	8.77	211	6	219.92
381	36.28	142.41	9.97	198	5	144.52
382	37.01	140.89	59.71	212	26	636.36
383	39.06	144.12	7.33	188	4	132.17
384	37.34	142.77	13.95	211	8	290.81
385	37.56	142.84	14.72	203	8	308.94
386	36.18	141.26	32.36	195	19	450.95
387	39.14	144.06	7.78	190	4	178.12
388	37.45	141.58	42.04	200	25	219.99
389	38.52	142.91	17.60	191	11	200.83

390	40.54	142.66	34.76	194	19	279.76
391	36.23	140.90	44.45	199	20	408.64
392	39.00	141.52	60.48	188	27	382.35
393	38.27	142.50	24.29	193	14	322.07
394	39.44	143.73	10.89	182	7	189.34
395	39.83	142.20	41.80	196	21	362.27
396	39.09	143.51	12.22	194	7	226.74
397	38.34	142.85	18.12	184	11	227.67
398	36.85	142.65	11.66	214	7	236.11
399	38.41	143.97	7.50	181	3	181.28
400	38.03	142.61	20.98	196	12	369.71
401	36.53	142.74	9.00	220	5	287.14
402	38.61	143.19	13.96	186	8	244.24
403	37.97	141.74	42.87	195	21	463.02
404	39.77	143.55	13.11	184	8	391.70
405	37.66	143.25	11.12	207	6	195.57
406	38.94	142.60	25.07	190	14	410.88
407	40.50	143.82	12.10	189	7	333.04
408	38.97	143.31	13.91	197	8	241.73
409	40.18	143.01	23.67	191	14	487.09
410	36.89	141.53	33.95	204	23	506.03
411	38.03	142.90	16.35	194	9	213.51
412	37.17	140.79	67.53	210	24	613.64
413	37.23	143.50	7.55	209	4	185.87
414	39.77	142.86	24.21	194	14	372.63
415	37.36	143.32	9.14	208	5	265.16
416	39.17	143.39	13.82	197	8	245.56
417	39.78	144.14	7.76	192	4	126.39
418	39.18	142.50	27.96	187	15	330.88
419	36.56	141.27	37.25	202	22	635.13

Fault Slip

	Strike-slip			Dip-slip		
Patch ID	Median	Mean	Standard deviation	Median	Mean	Standard deviation
1	2.08	2.14	4.62	2.40	2.40	5.16
2	-2.55	-2.54	6.13	7.82	7.92	8.02
3	-0.07	-0.03	6.22	3.32	3.59	6.89
4	-2.78	-2.76	6.18	9.33	9.63	9.53
5	-3.07	-3.07	5.13	0.94	1.07	5.28
6	-0.54	-0.53	5.65	10.82	11.09	9.70
7	0.48	0.48	6.24	11.52	11.80	10.52
8	2.05	2.02	6.21	1.76	2.11	6.28
9	-3.28	-3.32	5.98	-0.09	0.10	5.09
10	-1.76	-1.74	6.15	9.04	9.22	8.61
11	1.46	1.50	6.23	21.94	22.24	13.72
12	-0.02	0.02	6.56	5.76	6.18	8.51
13	1.34	1.32	6.16	4.87	5.05	7.00
14	0.34	0.32	4.60	0.35	0.42	4.58
15	-1.54	-1.55	5.91	4.21	4.29	6.03
16	-4.30	-4.30	5.15	0.70	0.81	5.26
17	-1.35	-1.34	6.31	13.84	13.87	9.35
18	-0.58	-0.58	6.00	6.69	6.79	7.16
19	-1.60	-1.59	6.17	12.14	12.17	8.85
20	-1.66	-1.61	5.88	6.81	6.94	7.62
21	3.48	3.48	6.34	6.71	6.89	8.24
22	-1.04	-1.04	6.42	5.44	5.73	8.15
23	3.59	3.57	6.07	4.53	4.93	7.90
24	1.94	1.93	5.06	1.39	1.45	5.06
25	-0.79	-0.77	3.85	1.07	1.06	4.37
26	-4.46	-4.41	5.58	-1.33	-1.10	4.60
27	-1.86	-1.82	5.50	-0.29	0.14	5.65
28	2.07	2.08	5.07	-4.20	-3.81	3.81
29	-0.46	-0.44	6.50	12.10	12.25	10.34
30	1.73	1.69	4.87	0.69	0.71	4.45
31	-1.67	-1.62	6.33	5.67	6.14	8.51
32	4.46	4.50	6.31	34.08	34.04	10.15
33	-0.66	-0.63	6.44	18.21	18.29	11.10
34	-0.30	-0.28	5.85	-1.80	-1.38	5.05
35	-3.95	-3.90	5.83	3.49	3.77	6.89
36	-1.46	-1.44	4.96	-1.87	-1.48	4.86
37	3.15	3.16	6.58	24.64	24.78	13.54
38	0.90	0.86	6.55	8.27	8.54	8.88

39	6.98	6.93	5.88	-0.43	-0.10	5.53
40	-0.69	-0.70	6.10	3.33	3.63	7.06
41	2.60	2.59	5.23	2.63	2.71	5.03
42	-5.39	-5.32	6.42	17.59	17.87	12.05
43	-1.05	-1.03	5.47	2.30	2.42	5.93
44	2.76	2.78	5.68	1.11	1.21	5.18
45	0.04	0.04	5.90	2.43	2.80	6.78
46	-0.05	-0.04	6.05	1.23	1.88	7.06
47	0.38	0.41	6.06	3.13	3.50	6.93
48	-2.61	-2.57	5.08	-0.23	0.05	5.07
49	-2.68	-2.69	6.20	-2.06	-1.89	4.11
50	0.69	0.69	5.09	-0.74	-0.48	5.24
51	-1.44	-1.47	5.73	-2.22	-1.86	4.70
52	0.46	0.45	5.99	5.32	5.53	7.60
53	0.25	0.25	6.07	13.25	13.47	10.83
54	-3.57	-3.58	4.53	1.06	1.16	4.88
55	2.21	2.18	5.59	5.97	6.07	6.79
56	-4.90	-4.84	6.37	1.35	1.74	6.62
57	-0.42	-0.43	6.20	1.97	2.32	6.67
58	1.65	1.68	6.11	0.78	1.31	6.50
59	-0.69	-0.71	5.63	-3.08	-2.56	4.59
60	1.71	1.76	6.39	15.38	15.42	9.78
61	-1.92	-1.91	4.93	-1.26	-1.02	4.76
62	0.60	0.60	6.73	47.76	47.61	12.84
63	0.49	0.47	6.02	-0.08	0.43	6.18
64	2.71	2.74	6.10	1.12	1.49	6.05
65	0.36	0.37	2.14	-1.34	-1.35	2.41
66	7.39	7.37	5.31	0.23	0.45	5.28
67	1.75	1.73	6.50	4.69	5.53	9.27
68	0.15	0.16	6.32	8.01	8.23	8.21
69	-0.26	-0.22	6.16	46.15	46.06	12.15
70	-0.80	-0.82	5.91	0.23	0.52	5.52
71	2.02	2.05	5.98	-0.90	-0.51	5.46
72	-0.53	-0.49	6.25	6.82	7.09	8.27
73	3.75	3.74	5.76	2.80	3.07	6.65
74	0.92	0.87	6.45	12.05	12.46	11.18
75	-3.58	-3.58	6.29	32.15	32.21	13.32
76	-2.80	-2.80	3.52	3.07	3.00	2.57
77	-1.91	-1.88	6.05	1.75	1.99	5.95
78	0.28	0.27	6.43	14.84	15.12	11.21
79	4.43	4.44	5.56	2.67	2.73	5.43
80	1.54	1.50	5.71	-4.15	-3.85	3.55
81	1.68	1.70	5.60	5.88	6.33	8.52
82	-3.78	-3.74	5.99	5.13	5.50	7.78

83	3.38	3.30	6.37	9.98	10.23	9.01
84	4.50	4.48	3.93	-0.04	0.01	4.33
85	2.80	2.79	5.16	5.99	6.28	7.87
86	0.88	0.85	6.25	2.81	3.25	7.27
87	1.86	1.85	6.17	-1.36	-0.85	5.39
88	-3.87	-3.86	6.18	15.54	15.70	10.63
89	0.94	0.96	6.29	38.52	38.50	13.85
90	2.98	3.01	6.23	3.68	3.92	6.68
91	-0.20	-0.23	6.31	-0.87	-0.38	5.66
92	1.92	1.95	5.24	3.60	3.61	5.90
93	1.78	1.81	5.42	0.64	0.80	5.19
94	-0.86	-0.89	5.23	9.10	9.12	6.88
95	0.52	0.50	6.69	2.91	3.15	6.58
96	2.45	2.42	6.09	1.25	1.42	5.84
97	-0.12	-0.13	5.63	-0.02	0.16	5.05
98	-0.28	-0.28	5.86	2.19	2.42	6.21
99	-1.86	-1.84	6.44	17.35	17.39	10.99
100	-4.31	-4.28	6.33	25.22	25.31	10.62
101	-5.25	-5.24	5.24	2.83	3.05	6.40
102	1.58	1.69	6.04	1.13	2.13	7.85
103	-3.60	-3.61	6.01	-1.23	-1.04	4.40
104	2.64	2.64	5.15	1.14	1.27	5.27
105	-0.79	-0.83	5.15	-0.29	-0.08	4.92
106	1.56	1.57	5.42	6.93	7.06	7.01
107	-1.69	-1.73	6.33	12.46	12.59	9.66
108	3.55	3.55	6.19	6.47	6.61	7.41
109	-3.80	-3.82	5.57	1.24	1.64	6.40
110	-1.66	-1.66	4.99	6.99	7.04	7.50
111	-1.94	-1.92	6.30	12.03	12.14	8.79
112	2.65	2.65	6.43	30.47	30.60	11.87
113	-0.11	-0.17	5.37	-0.67	-0.42	4.88
114	1.82	1.83	5.42	10.62	10.73	8.77
115	2.74	2.74	6.46	2.03	2.33	6.40
116	-0.67	-0.67	5.70	2.66	2.88	6.33
117	0.08	0.07	6.24	5.66	6.15	8.82
118	1.22	1.20	6.50	27.20	27.18	12.47
119	0.51	0.50	6.32	2.03	2.44	6.87
120	0.23	0.25	6.06	0.56	0.89	5.72
121	1.59	1.61	6.33	4.21	4.59	7.55
122	-1.91	-1.93	5.46	3.76	3.88	6.34
123	-3.20	-3.17	6.46	32.03	32.04	12.84
124	-0.69	-0.74	5.78	4.78	5.19	8.04
125	-0.43	-0.43	4.52	12.35	12.32	5.91
126	-3.86	-3.88	5.97	3.75	4.16	7.53

127	4.28	4.27	6.10	4.86	5.41	8.44
128	0.55	0.55	5.62	-1.70	-1.32	4.93
129	4.62	4.63	6.26	8.78	9.46	10.59
130	-3.03	-3.01	6.38	12.82	12.97	9.39
131	0.63	0.63	5.75	2.62	3.03	7.16
132	0.67	0.71	6.52	27.11	27.14	12.64
133	6.21	6.16	6.29	6.81	7.00	7.95
134	-2.18	-2.21	5.28	7.02	7.07	6.73
135	2.03	2.08	6.25	-0.15	0.21	5.61
136	1.84	1.85	6.43	1.78	2.21	6.64
137	-0.11	-0.15	6.29	13.64	13.76	9.12
138	-4.08	-4.07	6.51	18.52	18.74	11.94
139	2.81	2.85	6.31	18.28	18.49	12.73
140	1.69	1.70	6.24	10.01	10.67	11.12
141	-0.49	-0.46	6.18	15.54	15.73	10.94
142	3.37	3.40	6.40	3.26	3.59	7.09
143	3.19	3.10	6.25	9.61	9.83	8.81
144	-1.74	-1.74	5.60	3.24	3.48	6.55
145	-3.46	-3.41	4.86	0.09	0.37	5.18
146	-2.73	-2.76	6.06	13.13	13.11	7.99
147	0.70	0.72	5.41	9.44	9.54	8.44
148	-1.23	-1.24	6.67	13.73	13.94	11.32
149	1.83	1.86	6.31	5.39	5.52	7.10
150	3.21	3.23	5.84	10.39	10.49	8.48
151	0.24	0.23	6.33	15.99	16.09	11.09
152	1.33	1.33	6.00	6.41	6.63	7.53
153	0.84	0.80	6.24	9.69	10.34	11.18
154	0.97	0.94	5.76	-1.97	-1.68	4.75
155	-0.01	-0.02	6.27	12.41	12.44	8.80
156	3.57	3.62	6.07	-0.46	0.00	5.76
157	2.14	2.12	6.43	1.17	1.50	6.08
158	-0.62	-0.62	5.78	6.48	6.59	7.11
159	3.00	3.00	6.00	1.92	2.04	5.67
160	-0.64	-0.60	5.79	1.27	1.51	5.84
161	-5.59	-5.57	6.06	8.20	8.80	9.96
162	1.66	1.67	5.75	2.22	2.43	6.06
163	-0.22	-0.24	5.05	-1.07	-0.79	4.90
164	-1.51	-1.50	5.34	6.31	6.51	7.76
165	-0.78	-0.78	6.52	17.61	17.68	10.31
166	-0.23	-0.24	6.45	26.99	26.99	13.19
167	-1.93	-1.95	6.25	-2.53	-2.05	4.77
168	-0.28	-0.25	6.30	14.75	14.87	10.40
169	0.27	0.24	5.84	-3.83	-3.41	4.04
170	-0.02	0.01	5.78	-2.90	-2.57	4.16

171	4.80	4.79	6.27	36.22	36.25	11.69
172	-3.28	-3.23	5.40	1.70	1.90	5.70
173	6.22	6.19	6.08	-3.70	-3.08	4.55
174	5.23	5.25	6.22	2.67	3.25	7.64
175	3.70	3.70	5.83	1.88	2.06	5.89
176	-3.21	-3.23	5.75	0.58	0.72	5.20
177	2.02	2.05	5.77	2.98	3.28	6.76
178	-0.19	-0.22	5.00	-2.25	-2.03	4.32
179	1.96	1.95	6.25	29.13	29.14	12.14
180	2.32	2.27	6.23	11.82	11.90	9.09
181	-2.43	-2.45	5.58	2.03	2.34	6.52
182	-0.48	-0.48	6.10	14.56	14.51	9.03
183	4.39	4.33	6.36	51.03	51.14	12.97
184	1.74	1.74	5.91	5.69	6.23	8.90
185	-2.62	-2.58	6.35	0.47	1.04	6.48
186	-3.20	-3.17	5.90	-3.47	-3.20	3.76
187	-0.17	-0.23	6.31	15.69	15.81	10.69
188	-2.69	-2.72	5.66	-2.72	-2.41	4.30
189	-2.84	-2.82	6.28	20.49	20.68	13.05
190	2.33	2.33	6.07	-1.38	-0.84	5.54
191	3.08	3.08	5.81	0.43	0.99	6.39
192	-3.09	-3.07	6.31	6.22	6.49	8.04
193	-1.02	-0.95	6.61	44.53	44.51	11.15
194	4.39	4.39	5.16	4.17	4.29	6.32
195	-1.33	-1.35	3.17	-1.86	-1.85	3.37
196	-2.79	-2.84	4.50	3.00	3.03	5.57
197	2.41	2.40	2.12	-1.88	-1.86	1.90
198	-1.13	-1.07	6.29	17.27	17.32	10.39
199	4.29	4.26	6.35	14.12	14.19	9.65
200	-0.28	-0.25	6.39	24.71	24.91	14.03
201	0.64	0.71	5.02	-2.57	-2.29	4.28
202	1.23	1.28	6.22	28.21	28.18	12.34
203	3.11	3.10	6.47	11.28	11.47	9.40
204	2.11	2.10	6.21	4.95	5.49	8.44
205	1.15	1.18	6.14	20.50	20.60	12.12
206	-2.93	-2.94	6.21	6.91	7.25	8.98
207	-2.19	-2.21	6.30	18.78	18.91	10.12
208	-5.48	-5.48	5.85	2.48	2.56	5.56
209	-3.61	-3.59	6.17	1.76	2.15	6.59
210	7.51	7.48	5.53	-1.40	-1.11	4.76
211	-2.82	-2.76	6.49	25.50	25.47	10.20
212	1.03	1.04	6.08	32.71	32.80	14.08
213	-0.36	-0.35	6.55	17.23	17.33	10.04
214	0.54	0.54	5.20	1.84	1.90	5.19

215	-2.41	-2.38	6.39	0.64	1.10	6.34
216	-1.63	-1.66	6.35	6.17	6.51	8.08
217	-1.94	-1.94	6.45	19.34	19.36	9.50
218	6.18	6.13	6.21	13.81	13.72	8.15
219	1.41	1.35	6.24	19.67	19.95	13.01
220	-0.08	-0.05	6.11	16.68	16.87	12.30
221	2.97	2.97	6.09	0.16	0.51	5.77
222	-4.71	-4.74	6.25	14.37	14.45	10.39
223	1.98	2.02	6.16	15.47	15.46	10.09
224	0.39	0.40	3.74	-0.50	-0.47	3.82
225	-3.40	-3.38	5.28	-3.37	-3.01	4.15
226	-1.47	-1.48	6.23	21.52	21.64	12.60
227	-1.59	-1.58	5.51	0.37	0.51	5.17
228	-2.17	-2.15	5.51	8.36	8.49	7.47
229	-3.94	-3.92	6.28	3.78	4.07	7.39
230	1.89	1.88	5.62	1.17	1.53	6.18
231	2.86	2.93	6.30	11.25	11.41	9.70
232	-3.49	-3.47	5.98	13.25	13.23	8.98
233	1.99	1.99	5.93	16.04	16.25	10.97
234	1.91	1.90	4.70	-2.55	-2.44	3.73
235	-1.27	-1.25	5.75	1.83	2.11	6.22
236	3.52	3.50	5.99	-0.53	-0.14	5.46
237	-2.50	-2.52	5.41	9.20	9.32	8.13
238	-0.99	-1.02	6.02	1.66	2.37	7.38
239	-0.39	-0.41	6.39	12.77	13.01	10.56
240	0.16	0.18	6.36	21.80	21.81	12.08
241	3.25	3.26	3.50	-3.36	-3.21	3.39
242	2.45	2.42	6.21	9.57	9.67	8.22
243	4.75	4.73	6.21	12.05	12.29	10.02
244	2.11	2.14	5.96	-0.77	-0.44	5.29
245	-3.22	-3.22	6.17	24.75	24.80	12.98
246	-2.69	-2.62	6.42	28.01	28.02	11.00
247	-3.11	-3.11	5.52	-2.17	-1.80	4.76
248	0.66	0.67	6.42	20.09	20.26	12.76
249	0.65	0.60	5.51	-2.94	-2.71	3.99
250	7.16	7.13	5.95	6.06	6.37	7.81
251	1.72	1.75	6.45	13.04	13.33	11.12
252	3.84	3.84	6.19	25.09	25.02	12.53
253	-0.70	-0.71	5.99	12.28	12.42	9.49
254	2.27	2.19	6.28	-1.00	-0.56	5.50
255	0.28	0.32	6.12	2.85	3.09	6.84
256	2.25	2.25	6.36	13.19	13.30	8.90
257	-2.09	-2.13	6.26	6.79	6.94	7.99
258	4.89	4.85	5.21	1.96	2.09	5.74

259	4.93	4.88	5.45	-3.98	-3.58	3.91
260	-0.01	0.00	5.28	10.59	10.62	7.44
261	-1.01	-0.95	6.25	0.31	0.68	5.91
262	6.55	6.54	3.77	0.63	0.69	4.70
263	-4.23	-4.20	5.04	6.21	6.40	7.41
264	-2.28	-2.29	5.55	-0.04	0.31	5.61
265	-2.55	-2.53	5.83	-3.44	-2.93	4.45
266	3.81	3.79	6.02	18.10	18.13	9.76
267	3.99	4.01	5.82	3.32	3.53	6.76
268	-3.11	-3.12	6.20	20.39	20.34	9.09
269	-3.91	-3.87	5.98	1.01	1.19	5.42
270	0.56	0.58	6.09	2.85	3.07	6.24
271	5.00	4.97	6.41	6.91	7.71	10.21
272	3.11	3.09	5.69	2.81	2.91	5.76
273	0.81	0.78	6.26	15.98	16.05	9.91
274	-0.09	-0.11	4.60	-3.44	-3.19	3.75
275	-2.64	-2.61	6.24	1.85	2.17	6.50
276	-2.64	-2.61	6.30	27.15	27.19	9.67
277	-0.36	-0.36	5.77	-0.43	0.03	5.68
278	-1.57	-1.59	6.27	32.43	32.45	12.78
279	-1.66	-1.65	4.96	2.14	2.32	5.88
280	-4.88	-4.87	5.37	-0.61	-0.49	4.32
281	-0.03	0.00	6.05	17.20	17.24	9.78
282	1.27	1.29	6.24	38.25	38.14	13.43
283	1.27	1.25	5.04	6.67	6.73	7.24
284	1.00	1.01	6.43	7.59	8.11	9.88
285	2.69	2.67	5.26	-3.97	-3.82	3.25
286	1.87	1.84	6.27	7.91	8.42	10.02
287	3.39	3.39	6.29	32.67	32.72	11.79
288	6.27	6.24	6.11	15.55	15.78	11.45
289	-1.28	-1.23	5.95	11.25	11.33	8.53
290	0.48	0.52	5.74	2.05	2.22	5.96
291	-2.14	-2.06	6.68	29.30	29.23	11.10
292	-1.30	-1.30	5.72	8.14	8.25	8.02
293	-2.20	-2.19	5.87	1.43	1.81	6.58
294	0.13	0.11	6.00	-0.22	0.38	6.16
295	2.59	2.60	4.97	-2.32	-2.23	3.77
296	4.45	4.45	5.26	3.55	3.74	6.59
297	1.80	1.79	5.34	0.79	1.09	5.88
298	3.51	3.48	6.50	10.46	10.89	10.58
299	-2.39	-2.34	6.16	-3.23	-2.88	4.08
300	0.61	0.63	6.25	14.50	14.58	10.18
301	1.10	1.09	6.07	1.24	1.44	5.53
302	-2.96	-2.94	5.96	4.98	5.31	7.70

303	0.83	0.86	5.19	-0.69	-0.09	6.01
304	1.65	1.67	6.24	18.95	18.96	10.12
305	-1.10	-1.11	6.19	3.01	3.82	8.57
306	-0.43	-0.38	6.41	11.37	11.95	11.96
307	0.10	0.08	6.14	7.16	7.35	8.20
308	0.87	0.85	6.21	2.69	3.03	6.94
309	-1.85	-1.84	6.20	2.89	3.72	8.20
310	2.70	2.75	6.18	-3.57	-3.02	4.47
311	-0.88	-0.85	6.41	5.35	5.70	8.33
312	4.69	4.67	6.26	7.60	7.82	8.05
313	3.32	3.30	5.74	1.62	2.14	6.95
314	1.23	1.22	6.03	-0.19	0.19	5.63
315	1.31	1.30	6.21	10.79	11.20	10.41
316	6.29	6.28	6.51	47.95	47.96	12.23
317	-2.73	-2.74	3.46	2.00	1.99	4.16
318	-3.58	-3.56	6.37	7.33	7.67	8.86
319	2.14	2.12	6.28	1.23	1.78	6.78
320	3.40	3.37	5.95	-1.20	-0.74	5.38
321	-1.64	-1.64	6.43	4.02	4.26	7.10
322	3.04	3.05	5.45	6.01	6.14	7.10
323	-3.36	-3.29	5.17	-1.33	-1.06	4.73
324	0.77	0.77	6.26	19.15	19.28	12.20
325	-2.80	-2.79	6.13	0.53	1.23	6.99
326	5.76	5.76	3.99	0.62	0.68	4.48
327	0.91	0.90	5.34	2.82	2.99	6.36
328	1.07	1.07	6.36	26.11	26.03	11.77
329	1.92	1.93	6.21	21.53	21.46	10.56
330	0.55	0.53	5.93	5.31	5.87	8.77
331	1.18	1.18	5.11	1.60	1.89	6.07
332	4.01	4.01	5.71	0.91	1.32	6.43
333	0.12	0.10	6.78	27.67	27.87	12.63
334	-3.43	-3.42	5.91	9.19	9.33	8.37
335	1.00	1.00	6.50	5.28	5.49	7.60
336	1.83	1.75	6.41	17.79	18.25	13.40
337	0.78	0.84	5.92	2.87	3.13	6.34
338	-1.46	-1.41	5.88	4.52	4.69	6.82
339	-0.70	-0.67	6.38	37.48	37.56	13.52
340	-1.63	-1.62	3.86	2.00	2.02	4.50
341	3.94	3.93	6.16	1.88	2.13	6.16
342	-2.21	-2.16	5.93	-2.42	-2.02	4.60
343	0.72	0.67	5.43	-3.85	-3.34	4.23
344	1.59	1.53	6.00	1.92	2.19	6.38
345	3.06	3.07	6.57	32.34	32.31	11.86
346	5.32	5.25	6.46	9.25	9.49	9.29

347	3.07	3.09	6.02	-0.54	-0.15	5.58
348	-1.21	-1.22	5.93	0.37	0.70	5.82
349	0.65	0.62	6.44	8.29	8.78	9.99
350	0.40	0.39	5.96	2.61	3.01	6.92
351	-1.06	-1.04	5.62	1.06	1.55	6.62
352	-2.01	-1.99	5.71	2.50	3.03	7.39
353	1.66	1.65	6.16	3.51	3.71	6.52
354	-3.69	-3.71	4.08	2.06	2.10	5.26
355	1.02	1.01	5.37	2.46	2.55	5.54
356	2.38	2.39	6.30	14.75	14.97	11.52
357	-2.03	-2.03	6.35	0.39	0.64	5.73
358	-1.19	-1.21	6.05	1.06	1.30	5.75
359	3.54	3.49	6.49	47.50	47.43	13.54
360	2.69	2.69	4.67	-1.02	-0.86	4.69
361	-0.67	-0.63	6.41	12.24	12.43	10.15
362	0.59	0.59	2.33	-2.34	-2.34	2.59
363	1.00	1.00	6.05	10.39	10.36	7.72
364	0.04	0.05	6.36	7.57	7.97	9.04
365	1.60	1.62	6.23	5.35	5.50	7.33
366	3.41	3.43	6.34	1.06	1.43	6.30
367	6.43	6.42	5.53	4.00	4.10	6.41
368	0.98	0.96	6.24	19.80	19.86	11.95
369	4.36	4.31	6.28	-0.35	-0.04	5.38
370	0.97	0.97	5.47	1.51	1.93	6.43
371	1.10	1.11	6.35	33.89	33.93	12.87
372	-1.76	-1.76	5.43	-0.16	0.11	5.46
373	-3.24	-3.21	5.34	0.40	0.48	4.61
374	-8.65	-8.62	5.67	-4.29	-4.12	3.17
375	-0.29	-0.26	6.36	1.79	2.49	7.54
376	3.56	3.56	5.94	6.10	6.09	5.84
377	-0.77	-0.77	4.81	2.21	2.26	5.18
378	0.14	0.19	6.28	9.20	9.39	9.10
379	1.89	1.92	6.01	-2.51	-2.11	4.57
380	0.56	0.58	5.30	5.20	5.44	7.59
381	3.00	3.00	6.11	1.69	2.18	6.83
382	-2.31	-2.30	4.07	-1.19	-1.11	3.97
383	-1.06	-0.99	5.64	-0.17	0.46	6.28
384	-1.05	-1.01	6.22	23.43	23.46	10.74
385	1.91	1.86	6.27	38.65	38.64	11.20
386	-1.85	-1.89	6.21	-2.79	-2.47	4.24
387	3.89	3.89	5.46	2.53	2.85	6.53
388	-0.48	-0.49	6.66	1.85	2.35	7.10
389	-0.86	-0.88	6.30	39.93	39.88	13.64
390	1.42	1.36	6.13	-0.91	-0.55	5.29

391	1.28	1.30	4.62	-1.66	-1.44	4.54
392	1.66	1.72	5.17	0.49	0.73	5.65
393	1.45	1.45	6.25	28.65	28.67	13.61
394	1.49	1.47	6.05	2.83	3.16	6.86
395	-1.78	-1.81	5.67	-3.04	-2.63	4.42
396	2.01	2.06	6.42	6.18	6.34	7.37
397	2.83	2.83	6.62	47.46	47.47	15.28
398	-1.68	-1.63	6.04	7.11	7.25	7.59
399	1.80	1.84	5.69	3.41	3.62	6.50
400	-0.04	-0.03	6.20	52.72	52.62	12.95
401	1.38	1.35	5.35	4.99	5.36	8.06
402	3.58	3.53	6.26	28.60	28.54	11.09
403	-0.91	-0.96	6.01	1.89	2.41	7.34
404	-1.54	-1.56	6.24	6.28	6.51	7.99
405	-1.88	-1.87	6.36	5.75	6.12	7.98
406	1.35	1.32	6.42	12.25	12.56	10.42
407	-4.08	-4.10	5.95	12.32	12.40	8.50
408	8.36	8.31	6.46	35.35	35.29	11.29
409	1.09	1.12	6.01	-1.40	-1.04	5.02
410	-1.57	-1.59	6.22	0.12	0.31	4.99
411	0.45	0.44	6.28	59.82	59.70	13.87
412	-2.22	-2.20	3.31	-1.85	-1.82	3.41
413	-1.33	-1.28	5.39	8.47	8.56	7.56
414	2.38	2.39	6.48	2.01	2.57	7.09
415	-5.49	-5.52	5.91	5.90	6.15	7.51
416	-3.38	-3.38	6.59	13.69	13.80	10.08
417	-1.18	-1.15	5.70	7.11	7.31	7.92
418	-0.67	-0.66	6.30	13.50	13.68	10.37
419	-3.65	-3.68	5.19	-0.69	-0.53	4.85

References and Notes

1. C. DeMets, R. G. Gordon, D. F. Argus, Geologically current plate motions. *Geophys. J. Int.* **181**, 1 (2010). doi:10.1111/j.1365-246X.2009.04491.x

2. "Seismic Activity in Japan—Regional Perspectives on the Characteristics of Destructive Earthquakes (Excerpt)" (Earthquake Research Committee, Headquarters for Earthquake Research Promotion, Prime Minister's Office, Tokyo, 1998).

3. C. Hashimoto, A. Noda, T. Sagiya, M. Matsu'ura, Interplate seismogenic zones along the Kuril-Japan trench inferred from GPS data inversion. *Nat. Geosci.* **2**, 141 (2009). doi:10.1038/ngeo421

4. K. Minoura, F. Imamura, D. Sugawara, Y. Kono, T. Iwashita, The 869 Jogan tsunami deposit and recurrence interval of large-scale tsunami on the Pacific coast of northeast Japan. *J. Natural Disaster Sci.* **23**, 83 (2001).

5. See supporting material on *Science* Online.

6. S. E. Minson, M. Simons, J. L. Beck, paper presented at the AGU 2010 fall meeting, San Francisco, 13 to 17 December 2010, abstract G12A-02.

7. Y. Tanioka, T. Seno, Sediment effect on tsunami generation of the 1896 Sanriku tsunami earthquake. *Geophys. Res. Lett.* **28**, 3389 (2001). doi:10.1029/2001GL013149

8. A. Venkataraman, H. Kanamori, Observational constraints on the fracture energy of subduction zone earthquakes. *J. Geophys. Res.* **109**, B05302 (2004). doi:10.1029/2003JB002549

9. C. Vigny *et al*., The 2010 Mw 8.8 Maule Mega-Thrust Earthquake of Central Chile, Monitored by GPS. *Science* (2011). doi:10.1126/science.1204132 Medline

10. B. Delouis, J. M. Nocquet, M. Vallee, Slip distribution of the February 27, 2010 Mw=8.8 Maule Earthquake, central Chile, from static and high-rate GPS, InSAR, and broadband teleseismic data. *Geophys. Res. Lett.* **37**, L17305 (2010). doi:10.1029/2010GL043899

11. C. Ji, D. J. Wald, D. V. Helmberger, Source description of the 1999 Hector Mine, California, earthquake; Part II, Complexity of slip history. *Bull. Seismol. Soc. Am.* **92**, 1208 (2002). doi:10.1785/0120000917

12. S. Ni, H. Kanamori, D. Helmberger, Seismology: energy radiation from the Sumatra earthquake. *Nature* **434**, 582 (2005). doi:10.1038/434582a Medline

13. M. Ishii, P. M. Shearer, H. Houston, J. E. Vidale, Extent, duration and speed of the 2004 Sumatra-Andaman earthquake imaged by the Hi-Net array. *Nature* **435**, 933 (2005). Medline

14. R. Schmidt, Multiple emitter location and signal parameter estimation. *IEEE Trans. Antenn. Propag.* **34**, 276 (1986). doi:10.1109/TAP.1986.1143830

15. L. Borcea, G. Papanicolaou, C. Tsogka, Adaptive interferometric imaging in clutter and optimal illumination. *Inverse Probl.* **22**, 1405 (2006). doi:10.1088/0266-5611/22/4/016

16. Y. Zeng, J. G. Anderson, G. Yu, A composite source model for computing realistic synthetic strong ground motions. *Geophys. Res. Lett.* **21**, 725 (1994). doi:10.1029/94GL00367

17. T. H. Heaton, S. H. Hartzell, Estimation of strong ground motions from hypothetical earthquakes on the Cascadia subduction zone, Pacific Northwest. *Pure Appl. Geophys.* **129**, 131 (1989). doi:10.1007/BF00874626

18. H. Nakahara, Seismogram Envelope Inversion for High-Frequency Seismic Energy Radiation from Moderate-to-Large Earthquakes. *Adv. Geophys.* **50**, 401 (2008). doi:10.1016/S0065-2687(08)00015-0

19. M. Yamada, A. H. Olsen, T. H. Heaton, Statistical Features of Short-Period and Long-Period Near-Source Ground Motions. *Bull. Seismol. Soc. Am.* **99**, 3264 (2009). doi:10.1785/0120090067

20. A. A. Gusev, E. M. Guseva, G. F. Panza, Correlation between local slip rate and local high-frequency seismic radiation in an earthquake fault. *Pure Appl. Geophys.* **163**, 1305 (2006). doi:10.1007/s00024-006-0068-4

21. R. Madariaga, High-Frequency Radiation from Dynamic Earthquake Fault Models. *Ann. Geophys.* **1**, 17 (1983).

22. Y. Ito, K. Obara, K. Shiomi, S. Sekine, H. Hirose, Slow earthquakes coincident with episodic tremors and slow slip events. *Science* **315**, 503 (2007). doi:10.1126/science.1134454 Medline

23. A. Sladen *et al*., Source model of the 2007 M_w 8.0 Pisco, Peru earthquake: Implications for seismogenic behavior of subduction megathrusts. *J. Geophys. Res.* **115**, B02405 (2010). doi:10.1029/2009JB006429 Medline

24. Y. J. Hsu *et al*., Frictional afterslip following the 2005 Nias-Simeulue earthquake, Sumatra. *Science* **312**, 1921 (2006). doi:10.1126/science.1126960 Medline

25. J. Polet, H. Kanamori, Shallow subduction zone earthquakes and their tsunamigenic potential. *Geophys. J. Int.* **142**, 684 (2000). doi:10.1046/j.1365-246x.2000.00205.x

26. M. Cloos, Thrust-type subduction-zone earthquakes and seamount asperities: A physical model for seismic rupture. *Geology* **20**, 601 (1992). doi:10.1130/0091-7613(1992)020<0601:TTSZEA>2.3.CO;2

27. K. Mochizuki, T. Yamada, M. Shinohara, Y. Yamanaka, T. Kanazawa, Weak interplate coupling by seamounts and repeating M ~ 7 earthquakes. *Science* **321**, 1194 (2008). doi:10.1126/science.1160250 Medline

28. J. P. Loveless, B. J. Meade, Geodetic imaging of plate motions, slip rates, and partitioning of deformation in Japan. *J. Geophys. Res.* **115**, B02410 (2010). doi:10.1029/2008JB006248

29. H. Kanamori, M. Masatoshi, J. Mori, Investigation of the earthquake sequence off Miyagi prefecture with historical seismograms. *Earth Planets Space* **58**, 1533 (2006).

30. S. Y. Schwartz, Noncharacteristic behavior and complex recurrence of large subduction zone earthquakes. *J. Geophys. Res.* **104**, 23111 (1999). doi:10.1029/1999JB900226

31. K. Abe, Tectonic implications of the large Shioya-Oki earthquakes of 1938. *Tectonophysics* **41**, 269 (1977). doi:10.1016/0040-1951(77)90136-6

32. E. A. Hetland, M. Simons, Post-seismic and interseismic fault creep; II, Transient creep and interseismic stress shadows on megathrusts. *Geophys. J. Int.* **181**, 99 (2010). doi:10.1111/j.1365-246X.2009.04482.x

33. Y. Tanioka, K. Sataka, Fault parameters of the 1896 Sanriku tsunami earthquake estimated from tsunami numerical modeling. *Geophys. Res. Lett.* **23**, 1549 (1996). doi:10.1029/96GL01479

34. Z. Duputel *et al*., http://eost.u-strasbg.fr/wphase/events/tohoku_oki_2011 (2011).

35. J. F. Zumberge, M. B. Heflin, D. C. Jefferson, M. M. Watkins, F. H. Webb, Precise point positioning for the efficient and robust analysis of GPS data from large networks. *J. Geophys. Res.* **102**, 5005 (1997). doi:10.1029/96JB03860

36. W. Bertiger *et al*., Single receiver phase ambiguity resolution with GPS data. *J. Geod.* **84**, 327 (2010). doi:10.1007/s00190-010-0371-9

37. J. P. Davis, R. Smalley Jr., Love wave dispersion in central North America determined using absolute displacement seismograms from high-rate GPS. *J. Geophys. Res.* **114**, B11303 (2009). doi:10.1029/2009JB006288

38. F. Gonzalez, H. B. Milburn, E. N. Bernard, J. Newman, (1998), in Proceedings of the International Workshop on Tsunami Disaster Mitigation, 19 to 22 January 1998, Tokyo (http://nctr.pmel.noaa.gov/dart_report1998.html).

39. W. H. F. Smith, D. T. Sandwell, Global sea floor topography from satellite altimetry and ship depth soundings. *Science* **277**, 1956 (1997). doi:10.1126/science.277.5334.1956

40. N. Takahashi *et al*., Seismic sructure and seismogenesis off Sanriku region, northeastern Japan. *Geophys. J. Int.* **159**, 129 (2004). doi:10.1111/j.1365-246X.2004.02350.x

41. S. E. Minson, thesis, California Institute of Technology (2010).

42. C. Ji, D. V. Helmberger, D. J. Wald, K. F. Ma, Slip history and dynamic implications of the 1999 Chi-Chi, Taiwan, earthquake. *J. Geophys. Res.* **108**, 2412 (2003). doi:10.1029/2002JB001764

43. C. Bassin, G. Laske, G. Masters, The current limits of resolution for surface wave tomography in North America. *Eos Trans. AGU* **81**, F897 (2000).

44. J. C. VanDecar, R. S. Crosson, Determination of teleseismic relative phase arrival times using multi-channel cross-correlation and least squares. *Bull. Seismol. Soc. Am.* **80**, 150 (1990).

45. P. Goldstein, R. J. Archuleta, Deterministic frequency-wavenumber methods and direct measurements of rupture propagation during earthquakes using a dense array: Theory and methods. *J. Geophys. Res.* **96**, 6173 (1991). doi:10.1029/90JB02123

46. J. B. Fletcher, P. Spudich, L. M. Baker, Rupture propagation of the 2004 Parkfield, California, earthquake from observations at the UPSAR. *Bull. Seismol. Soc. Am.* **96**, S129 (2006). doi:10.1785/0120050812

47. Y. Suwa, S. Miura, A. Hasegawa, T. Sato, K. Tachibana, Interplate coupling beneath NE Japan inferred from three-dimensional displacement field. *J. Geophys. Res.* **111**, B04402 (2006). doi:10.1029/2004JB003203